Perspectives on Moist Baroclinic Instability: Implications for the Growth of Monsoon Depressions

NAFTALI Y. COHEN AND WILLIAM R. BOOS

Department of Geology and Geophysics, Yale University, New Haven, Connecticut

(Manuscript received 26 August 2015, in final form 6 January 2016)

ABSTRACT

Little is known about the genesis and growth mechanisms of monsoon depressions, despite the great importance of these storms for the hydrological cycle of the Asian–Australian monsoon region. Of the few theoretical studies that have examined this issue, most have attributed the amplification of monsoon depressions to some form of baroclinic instability or stable baroclinic growth, highly modified by the diabatic effects of moist convection. Here, a simple criterion—namely, the upshear tilt of potential vorticity anomalies—is argued be necessary for dry or moist baroclinic growth. Reanalysis data are then used to assess whether a large ensemble of South Asian monsoon depressions has vertical structures consistent with this criterion. The evolution of these monsoon depressions is compared with that of ensembles of hurricanes and diabatic Rossby waves, the latter being prototypical examples of moist baroclinic instability. During their amplification phase, monsoon depressions do not exhibit an upshear tilt of potential vorticity anomalies. Many similarities are found between developing monsoon depressions and hurricanes but few with diabatic Rossby waves. Thus, the mechanism responsible for the intensification of monsoon depressions remains unknown, but these results indicate greater similarity with the general process of tropical depression spinup than with moist convectively coupled baroclinic instability.

1. Introduction

Like Earth's midlatitude troposphere, the South Asian and Australian monsoons contain baroclinic zones with strong vertical shear in which synoptic-scale cyclones grow. These low pressure systems produce a large fraction of the total monsoon precipitation received by India and northern Australia (Ding and Sikka 2006; Yoon and Chen 2005; Hurley and Boos 2015). They typically have outer diameters of about 2000 km, extend through the full depth of the troposphere, and propagate westward and poleward at speeds of a few meters per second (Sikka 1977; Hurley and Boos 2015).

Occurrences of these synoptic-scale low pressure systems have traditionally been called ''monsoon depressions'' (MDs) when their surface wind speeds fall in the range of 8.5–13.5 $m\,s^{-1}$ or when their surface pressure minima fall below that of their surroundings by 4–10 hPa (India Meteorological Department 2011; Ajayamohan et al. 2010). Weaker vortices with similar length scales are called ''monsoon lows,'' and stronger vortices are called ''deep depressions'' or ''cyclonic storms.'' Indian MDs typically have a tilt in the vertical to the west and south, a warm-over-cold temperature anomaly in their center, and locally cyclonic vorticity that extends from the surface to the upper troposphere with peak horizontal winds around 700–800 hPa (e.g., Godbole 1977).

After formation, Indian MDs propagate to the northwest, upstream relative to the lower-tropospheric flow in which they are embedded, and have an average lifetime of about 10 days (Fig. 1 and Table 3). It was recently shown that the upstream propagation is largely adiabatic and is produced by horizontal, nonlinear advection (Boos et al. 2015). About six MDs form during each summer, on average, in the Indian monsoon domain. Some studies (e.g., Rajendra Kumar and Dash 2001) have found a downward trend over the past few decades in the number of MDs recorded each summer by the India Meteorological Department (IMD), but Cohen and Boos (2014) showed that this trend may not be robust owing to problems with the underlying dataset.

Corresponding author address: Naftali Y. Cohen, Lamont-Doherty Earth Observatory, 205B Oceanography, 61 Route 9W, Palisades, NY 10964.
E-mail: ncohen@ldeo.columbia.edu

DOI: 10.1175/JAS-D-15-0254.1

© 2016 American Meteorological Society

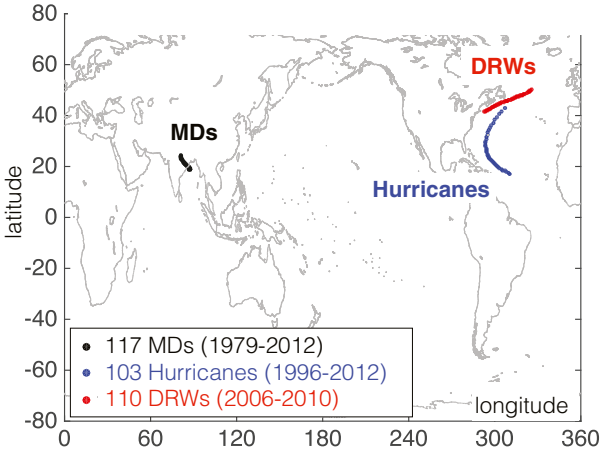

FIG. 1. Ensemble-mean tracks of disturbances examined in this study: monsoon depressions (black), Atlantic hurricanes (blue), and diabatic Rossby waves (red). To obtain these mean tracks, we first interpolate every storm in time to a 10-day period and then average the locations of storm centers over all storms within each ensemble.

Only a handful of studies have investigated the mechanisms responsible for the genesis and amplification of MDs. Nearly all such studies were conducted in the 1970s or 1980s and invoked barotropic instability, baroclinic instability, or nonmodal baroclinic growth, with some modification by precipitating convection. Given that MDs grow in an environment with strong vertical shear, strong horizontal shear, and abundant moisture, all of these mechanisms would seem to merit consideration. We now discuss each briefly.

Early linear stability analyses of the observed time-mean flow over South Asia found barotropic instabilities to be limited to the upper troposphere and to have little resemblance to observed MDs (Shukla 1977; Goswami et al. 1980). But then Lindzen et al. (1983) showed that the time-mean Indian monsoon flow was barotropically unstable if finite-amplitude initial perturbations were considered, with the local easterly maximum at 500 hPa over the Bay of Bengal in July producing a most unstable mode with a horizontal wavelength of 2600 km and a westward phase speed of 1.5 m s^{-1}. Although these length and velocity scales are realistic, barotropic dynamics alone cannot explain the strong vertical motions and horizontal temperature gradients found in observed MDs (e.g., Krishnamurti 1985). Furthermore, the generation of disturbance energy by diabatic processes is much larger than that by barotropic exchanges (Krishnamurti et al. 1976); one recent study even found that the barotropic energy of MDs is converted to the barotropic energy of the mean state (Krishnamurti et al. 2013), which would rule out barotropic instability as a growth mechanism. We conclude that even if barotropic dynamics play some role in the very early stages of development of MDs, baroclinic or moist diabatic processes must be responsible for most of the amplification.

Multiple studies have examined whether Indian MDs could result from baroclinic instability of the time-mean flow. Dry baroclinic instability in the easterly shear that characterizes monsoons requires a larger shear amplitude than in westerly shear, otherwise the interior meridional gradient of potential vorticity (PV) will be positive and the Charney and Stern (1962) necessary criterion for baroclinic instability will not be satisfied [see discussion by Moorthi and Arakawa (1985)]. The critical value of easterly shear needed to satisfy this criterion is about $-6.8\,\mathrm{m\,s^{-1}\,km^{-1}}$, which is larger than is commonly observed in monsoons (Wang 1990). Dry, linear analyses of the observed mean flow over South Asia have found that although baroclinic and combined barotropic–baroclinic instabilities exist in parts of the domain, the characteristics of these instabilities differ considerably from those of observed MDs (e.g., Goswami et al. 1980; Mishra and Salvekar 1980). Thus, dry baroclinic instability does not seem to be a likely growth mechanism.

It is possible that MDs could result from transient baroclinic growth even though the flow has no unstable normal modes, as noted by Farrell (1985). A key issue, then, is whether observed structures are consistent with such hypothesized mechanisms of baroclinic growth. Cyclones growing by baroclinic processes are expected to tilt upshear, but with the exception of just a few studies (e.g., Saha and Chang 1983), most analyses find that MDs tilt downshear (Godbole 1977; Keshavamurty et al. 1978; Douglas 1992). However, it is possible that these studies have examined the mature or decaying phase of individual MDs and that these storms do tilt upshear during their growth phase. To our knowledge, a comprehensive analysis of the vertical structure of a large sample of MDs throughout their life cycle has not been conducted.

Precipitation is abundant in MDs, as noted above, so any sort of baroclinic growth process is likely to be greatly modified by the diabatic effects of precipitating convection. This was recognized in early studies of the baroclinic stability of the monsoon circulation, with several authors altering their linear stability analyses to include either a moisture-convergence closure or a quasi-equilibrium closure for precipitating convection (e.g., Shukla 1978; Mak 1983). Addition of these convection parameterizations greatly modified the results in ways that were highly sensitive to the details of the parameterization, with some treatments producing unstable modes that had wavelengths, phase speeds, and

vertical structures that were argued to be consistent with observations of MDs (Moorthi and Arakawa 1985). Moist baroclinic instability continues to be one of the leading explanations for the growth of Indian MDs, to the extent that this topic is even discussed in recent literature (e.g., Krishnakumar et al. 1992; Parija and Dash 1995; Krishnamurti et al. 2013). However, previous analyses of moist baroclinic instability in easterly shear were all limited to linear, normal-mode analyses. This is unfortunate because the fully nonlinear, transient structures that develop during moist baroclinic growth in westerly shear have been shown to differ substantially from those predicted by linear, normal-mode analyses (Moore and Montgomery 2004). Yet, we will argue in the next section of this paper that, regardless of the sign of the vertical shear, the PV of the disturbance must have a vertical tilt that is in the opposite direction of the vertical shear vector in order for moist or dry baroclinic instability to produce disturbance growth.

The goal of this paper is to determine whether modern observations of a large number of Indian MDs are consistent with existing theories for moist baroclinic growth. Whereas many previous studies examined the development of MDs using simplified models (e.g., multilevel quasigeostrophic models or linear stability analyses) to establish consistency with observed bulk measures of MD size or propagation speed, here we use reanalysis data to study the observed evolution of an ensemble of storms and compare with a few theoretical metrics. We concentrate our attention on observed vertical structures and the necessary conditions for moist baroclinic growth, with a particular focus on the early part of the storm life cycle during which amplification occurs.

We begin in the next section by reviewing the theory and necessary conditions for moist baroclinic instability. Previous literature has identified multiple mechanisms by which precipitating convection and basic-state baroclinicity can interact to produce disturbance growth, and we show that all of these can be identified in observations using a simple criterion based on the vertical structure of PV. Section 3 then describes the data and methods used in our analyses of ensembles of MDs, hurricanes, and diabatic Rossby waves (DRWs). In section 4, we present our main results, focusing on the anomalous PV and temperature fields as they evolve over the course of storm lifetimes. As will be shown, we expect PV anomalies to lean against the mean vertical shear in order to transfer energy from the mean baroclinicity to perturbation development. This process, as we will show, is not observed in MDs and hurricanes, while it is observed clearly during the spinup of DRWs. We close with a summary of our results and a discussion of their implications.

2. A conceptual review of moist baroclinic instability

Two perspectives can be used to understand the classical mechanism of baroclinic instability: a PV perspective that focuses on the interaction of PV anomalies at different vertical levels or an energetic perspective that focuses on the process by which perturbations draw energy from the environmental available potential energy (Grotjahn 2003). Here we use the same two perspectives to review existing theories of moist baroclinic growth and to establish a diagnostic criterion that will be used in the remainder of this paper. We consider this discussion necessary because multiple studies have examined how moist convection can interact with the baroclinicity of a basic state to produce disturbance growth, but the similarity between the mechanisms they describe is unclear, as are the criteria one could use to compare their predictions with observations (e.g., Shukla 1978; Moorthi and Arakawa 1985; Snyder and Lindzen 1991; Montgomery and Farrell 1991; Moore and Montgomery 2004). Although our discussion of the PV perspective focuses on unstable linear normal modes, our review of the energetic perspective addresses disturbance amplification through transient stable, nonmodal growth.

a. *Potential vorticity perspective*

This view uses a Rossby wave perspective to understand baroclinic instability and dates back to Lighthill (1963) and Bretherton (1966) but was recently reviewed and generalized by Heifetz et al. (2004). In short, it was argued that dry baroclinic instability can be interpreted as an interaction between a pair of counterpropagating Rossby waves (CRWs): one with PV anomalies focused where the PV meridional gradient is positive and one where it is negative. Usually these locations are around the tropopause and the ground. The interaction and mutual growth of both Rossby waves are mediated by the meridional velocity that each wave induces on the other. Recently, de Vries et al. (2010) generalized this framework to include moisture; here we essentially summarize but also simplify their results and then use them to devise a straightforward necessary criterion for moist baroclinic growth that can be applied to observations.

The analog of PV in the quasigeostrophic framework, which we use for this discussion, is the pseudopotential vorticity $q = \zeta_g + f_0 b_z N^{-2}$, where b is the buoyancy, N is the buoyancy frequency, ζ_g is the vorticity of the geostrophic wind, and f_0 is a constant Coriolis parameter. This quantity is advected by the geostrophic wind (u_g, v_g) and has sources and sinks associated with the vertical gradient of the diabatic heating H:

$$D_g q = q_t + u_g q_x + v_g q_y = \frac{f_0}{N^2} H_z. \tag{1}$$

We linearize this conservation equation about a time-mean flow that is purely zonal, yielding

$$\overline{D}_g q' + v'\overline{q}_y = q'_t + \overline{u}_g q'_x + v'\overline{q}_y = \frac{f_0}{N^2} H'_z, \tag{2}$$

where $\overline{D}_g = \partial/\partial t + \overline{u}_g \partial/\partial x$, and an overbar denotes mean quantities while a prime denotes deviations from the mean. Henceforth, we omit the primes as well as the subscript g with the understanding that all quantities without primes are anomalies and all horizontal winds are geostrophic.

A key assumption here is that, in the presence of moisture, PV anomalies can be linearly partitioned[1] into "dry" and "moist" components (de Vries et al. 2010). For example,

$$q = q^{(d)} + q^{(m)}. \tag{3}$$

The dry component $q^{(d)}$ is related to meridional parcel displacements[2] while the moist component $q^{(m)}$ is generated by vertical gradients in the diabatic heating. Hence, using (3) in (2) yields

$$q_t^{(d)} + \overline{u} q_x^{(d)} = -v\overline{q}_y \quad \text{and} \tag{4}$$

$$q_t^{(m)} + \overline{u} q_x^{(m)} = \frac{f_0}{N^2} H_z. \tag{5}$$

A second key assumption is that the diabatic heating H can be parameterized in terms of the vertical velocity w,

$$H = \varepsilon_1 w r(z) \quad \text{such that} \quad H_z \simeq \varepsilon_1 w r_z(z), \tag{6}$$

where r is a horizontally invariant moisture profile, ε_1 is a dimensionless amplitude, and $w = w(x, y, z, t)$. This is a so-called large-scale rain parameterization in which condensation occurs during stable lifting and is proportional to the rate of lifting and the amount of moisture present at a given level. The solutions are sensitive to the vertical structure chosen for r (e.g., Moore and Montgomery 2004), but here we simply think of PV being diabatically altered at the top and bottom of a uniformly moist layer (i.e., the cloud layer above the lifted condensation level) so that the vertical gradient in H is dominated by the vertical gradient in moisture.[3]

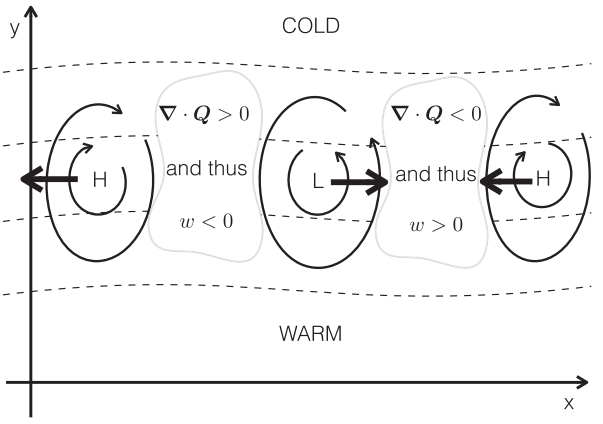

FIG. 2. Schematic solution to the quasigeostrophic omega equation [see (7)] for a train of cyclones and anticyclones in a climatological negative meridional temperature gradient. Thin curved arrows show the geostrophic wind, dashed lines show isotherms, and thick arrows show **Q** vectors. This figure is based on Fig. 3 in Sanders and Hoskins (1990).

The vertical velocity can be obtained diagnostically from the quasigeostrophic omega equation (e.g., Holton and Hakim 2013),

$$\nabla^2 w \propto \nabla \cdot \mathbf{Q}, \tag{7}$$

where if the mean (potential) temperature gradient $\overline{\theta}_y < 0$ then $\mathbf{Q} = -gN^{-2}\theta_0^{-1}|\overline{\theta}_y|\hat{\mathbf{k}} \times \partial \boldsymbol{v}_g/\partial \mathbf{x}$ where θ is the potential temperature, θ_0 is some reference temperature, g is the gravitational acceleration, $\hat{\mathbf{k}}$ is the local unit vertical vector, and $\boldsymbol{v}_g$ is the horizontal geostrophic wind vector. Figure 2 illustrates a family of cyclones and anticyclones in a region where the x axis follows the isotherm and thus where there is westerly vertical shear. Ascent occurs on the downshear (east) side of cyclones while subsidence occurs on the upshear side. This diagnostic coupling between vertical motion and geostrophic vorticity provides the mechanism by which the

[1] A full account for a general initial condition can be made by adding a passive PV to the linear partition in (3). The passive PV represents remnant values generated by past diabatic processes. This is discussed in de Vries et al. (2010) but omitted here for the sake of simplicity.

[2] That is, $q^{(d)} = -\eta\overline{q}_y$. This follows as $\overline{D}q^{(d)} = -v\overline{q}_y$ as in (4) and $\overline{D}\eta = v$, where η is the meridional displacement. Hence, $\overline{D}q^{(d)} = -\overline{q}_y\overline{D}\eta = -\overline{D}(\eta\overline{q}_y)$, and $q^{(d)} = -\eta\overline{q}_y$ after integration in time.

[3] An alternate treatment specifies H as a function of w at cloud base (i.e., in the lower troposphere), and we call this treatment a "cumulus parameterization" because it is similar in spirit to schemes that scale the convective mass flux with the low-level mass convergence. De Vries et al. (2010) found that the both cumulus and large-scale rain parameterizations produced similar unstable diabatic Rossby wave modes, but only the cumulus parameterization produced unstable "moist instability" and "tropopause intrusion" modes. This is of little concern here because we are interested in the transient growth of stable modes in addition to the usual modal instabilities.

TABLE 1. Possible unstable interactions between PV components. All PV anomalies can be associated directly ($\rightarrow$) with v by inversion and with w via the omega equation. Then v can alter dry PV through meridional advection and w can provide a source of moist PV by diabatic heating. Note that $q^{(d)}$ and $q^{(m)}$ in the diabatic Rossby wave refer to PV in the bottom and upper middle layer, respectively, while $q^{(d)}$ and $q^{(m)}$ in the tropopause intrusion refer to PV in the top and bottom middle layer. All interactions are cyclic.

Interaction type	Way of interaction
Dry instability	$q^{(d)} \rightarrow v \rightarrow q^{(d)}$
Moist instability	$q^{(m)} \rightarrow w \rightarrow H \rightarrow q^{(m)}$
Diabatic Rossby wave	$q^{(d)} \rightarrow w \rightarrow H \rightarrow q^{(m)} \rightarrow v \rightarrow q^{(d)}$
Tropopause intrusion	$q^{(m)} \rightarrow v \rightarrow q^{(d)} \rightarrow w \rightarrow H \rightarrow q^{(m)}$

source term H_z is coupled to both the dry and moist components of PV. Note that w is set entirely by dry adiabatic processes and diabatic heating is not influenced by horizontal moisture advection, wind-dependent surface evaporation, etc. Indeed, moisture is not prognostic in existing analytical theories of moist baroclinic instability (e.g., Emanuel et al. 1987; Montgomery and Farrell 1991; Moore and Montgomery 2004; de Vries et al. 2010), which shows that there is ample room for future theoretical development.

We now use the fact that, in the quasigeostrophic system, the pseudo-PV anomalies can be inverted and the velocities associated with each component can be linearly superimposed. That is,

$$\boldsymbol{v} = \boldsymbol{v}^{(d)} + \boldsymbol{v}^{(m)} \quad \text{and} \quad w = w^{(d)} + w^{(m)}, \tag{8}$$

and recall that $q^{(d)}$ is altered by v as in (4) while $q^{(m)}$ is altered by w (or H) as in (5). Thus, although H does not influence the dry PV in (4) directly, it does influence it indirectly through advection by the meridional velocity $\boldsymbol{v}^{(m)}$ associated with the moist PV. Similarly, the dry PV is associated with vertical velocity $w^{(d)}$, via the omega equation, which provides a diabatic source for the moist PV $q^{(m)}$. Moist and dry PV components can thus interact with each other as well as evolve independently. Table 1 details four possible ways in which the dry and moist PV can interact to produce instability, as will be discussed below.

While it is intuitive that PV changes must be accompanied by meridional wind changes and vice versa by PV inversion, the relationship between PV and vertical velocity is perhaps less obvious. Here we present a new and simple way to view that relation, based on the fact that vertical motions of a single sign reside within zonal PV dipoles (e.g., Fig. 2). We argue that w can be parameterized in terms of q_x, and using (7) we obtain, as an approximation,

$$w = \mathrm{sgn}(\overline{\theta}_y)\frac{\varepsilon_2 g L}{N^2} q_x, \tag{9}$$

where ε_2 is a second dimensionless amplitude parameter and L is a horizontal scale. For now we assume $\overline{\theta}_y < 0$ and hence $w = -\varepsilon_2 g L N^{-2} q_x$.

The evolution and interaction of PV components can be better understood by viewing each anomaly as part of a Rossby wave. To accomplish this, we note that $(u, v) \equiv (-\psi_y, \psi_x)$, where ψ is a streamfunction and $q = \nabla^2\psi$, which will be used to represent the advection of q by the horizontal wind in our wave equations. The phase speeds of noninteracting waves in $q^{(d)}$ and $q^{(m)}$ can be obtained by assuming one-dimensional normal modes with zonal wavenumber k and frequency $\omega = kc_p$, where c_p is an intrinsic phase speed. Assume that initially $\phi = \phi(x, t)$ for some generic variable ϕ, and a normal-mode pattern exists such that

$$\phi = \phi_k \exp ik(x - ct). \tag{10}$$

Substitution of (10) in (4) and (5) then yields the phase speeds of waves in $q^{(d)}$ and $q^{(m)}$, respectively:

$$c_p^{(d)} = \overline{u} - \frac{1}{k^2}\overline{q}_y \quad \text{and} \quad c_p^{(m)} = \overline{u} + \frac{\varepsilon f_0 g L}{N^4} r_z. \tag{11}$$

Here we used the relations $v_k = ik\psi_k = -iq_k/k$ and, from (9), $w_k = -ik\varepsilon_2 g L N^{-2} q_k$. In addition, $\varepsilon = \varepsilon_1\varepsilon_2$. Hence, the dry wave's phase speed and direction are set by the mean PV gradient (as expected for a classical Rossby wave), while the moist wave's intrinsic phase speed and direction are set by the vertical gradient of diabatic heating.

We find it helpful to regard the moist wave in the second equation in (11) as a Rossby wave in which the vertical gradient of diabatic heating acts as an "equivalent" PV gradient. More precisely, we set the second term on the right-hand side of the second equation in (11) equal to $k^{-2}\overline{q}_y^*$, where the equivalent PV gradient[4]

$$\overline{q}_y^* = -(\varepsilon f_0 g L N^{-4}) r_z k^2. \tag{12}$$

Then the intrinsic moist phase speed can be written

$$c_p^{(m)} = \overline{u} - \frac{1}{k^2}\overline{q}_y^*, \tag{13}$$

[4] Integrating (12) meridionally yields an equivalent PV with an equator-to-pole gradient on which the moist wave propagates. While this is a mathematical trick and is not meant to imply the existence of a physical quantity with a meridional gradient, it encapsulates the combined effects of the meridional temperature gradient needed to produce quasigeostrophic ascent [as described in (9)] and the vertical moisture gradient that turns ascent into a diabatic PV source that in turn causes wave propagation [as described in the second equation in (11)].

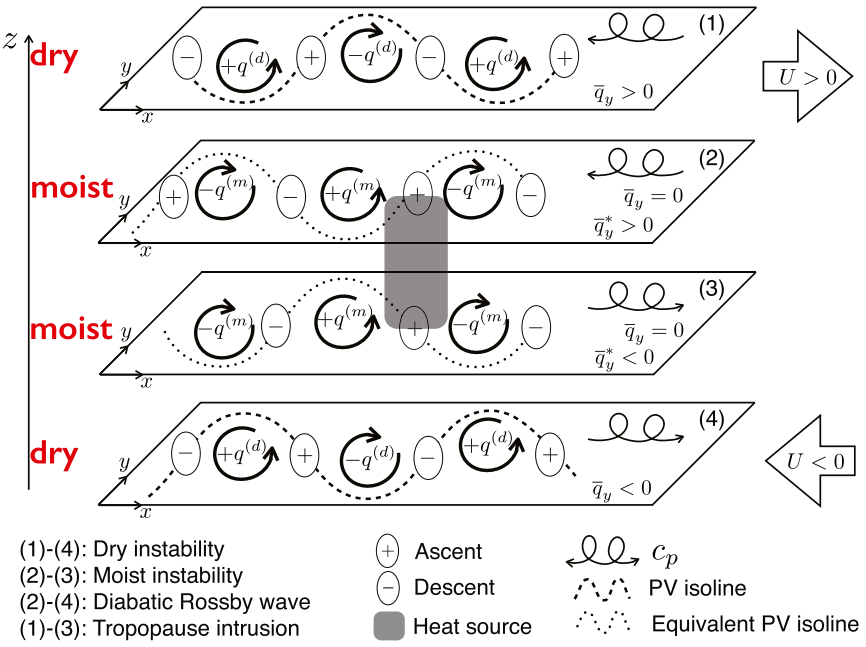

FIG. 3. Schematic of dry and moist PV components in counterpropagating Rossby waves. Four vertically stacked, horizontal layers on an f plane are shown in a basic state with positive vertical shear $\overline{u}_z > 0$. In each layer a wave train of cyclones and anticyclones is shown with the corresponding perturbation PV (dashed and dotted lines are isolines of total dry and moist PV, respectively). Perturbations are assumed to be normal modes and to be accompanied by vertical motions in accordance with the quasigeostrophic omega equation (ellipses enclosing positive and negative signs represent ascent and descent, respectively). Moist convective diabatic heating is shown as a vertical gray rectangle. The direction of zonal propagation relative to the basic-state flow is shown by the curly arrows. The four possible unstable interactions are noted in the bottom left.

allowing us to use concepts from the dry instability model of CRWs (e.g., Heifetz et al. 2004) to describe the action of moist processes.

We now discuss how instability can arise from interactions involving only $q^{(d)}$, only $q^{(m)}$, or both $q^{(d)}$ and $q^{(m)}$. These categories of interaction were discussed in a rigorous mathematical framework by de Vries et al. (2010), while here we provide a conceptual summary and note the PV structures that are required for instability in each case. The conceptual model in which all these interactions can occur has four fluid layers and is illustrated in Fig. 3. It consists of an f plane with basic-state flow $\overline{u} = \overline{u}(z)$ and constant positive shear so that $\overline{T}_y < 0$ by thermal wind balance (in the appendix we consider the scenario of constant negative shear). More importantly, there are no PV gradients in the interior (as $\overline{u}_{zz} = \overline{u}_{yy} = 0$), but $\overline{q}_y < 0$ in the bottom layer and $\overline{q}_y > 0$ in the top layer. We assume that moisture is abundant in the model interior (the two middle layers) so that the vertical motions that are in quadrature with any PV anomalies (see Fig. 2) are accompanied by latent heating. This diabatic heat source has the vertical structure $wr(z)$ and is illustrated by the gray rectangle in the center of Fig. 3. At the top of the region in which diabatic heating occurs $r_z < 0$, while at the bottom $r_z > 0$. This motivated the construction of the two middle layers that lie above and below the diabatic heating maximum and have equivalent PV gradients of $\overline{q}^*_y > 0$ and $\overline{q}^*_y < 0$, respectively.

Each layer independently supports the propagation of zonally propagating edge waves. Classic dry Eady edge waves propagate in opposite directions and against the mean flow in layers 1 and 4, assuming $\overline{u}$ is shifted by a barotropic wind so that the vertical shear gives opposing mean winds in those two layers. At the top and bottom of the diabatically heated region (layers 2 and 3, respectively), $\overline{q}^*_y$ is of opposite sign, thus by the second equation in (11) these moist edge waves also propagate in opposite directions and against the mean flow. Physically, these moist edge waves propagate in opposite directions because the diabatic heating produces a positive PV anomaly below and negative PV anomaly above (according to the sign of r_z and the induced w) and this corresponds to an eastward shift of PV in the

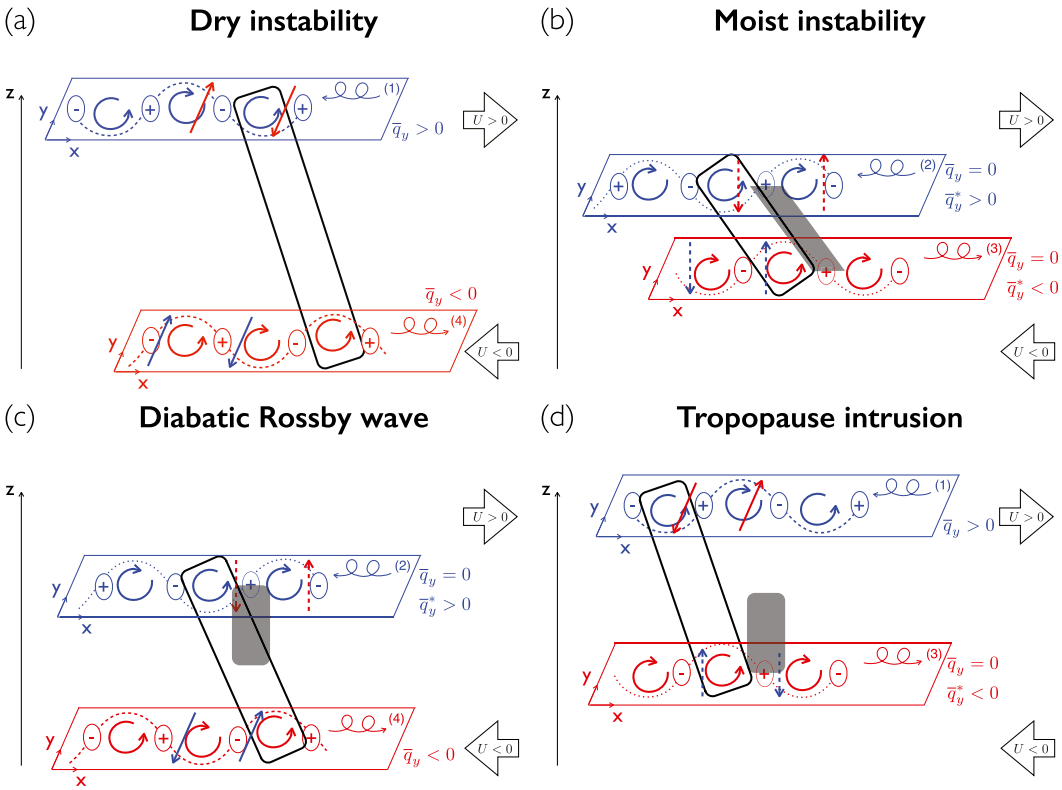

FIG. 4. Schematics of the four possible unstable interactions between counterpropagating Rossby waves, with symbols as described in Fig. 3. Black rectangles surround tilted columns of cyclonic PV, illustrating that the anomalous PV (or streamfunction) must lean against the shear in order for instability to occur. (a) The dry model, as in Heifetz et al. (2004), (b) the fully moist instability case, (c) the diabatic Rossby wave case, and (d) the tropopause intrusion case. In addition, in each panel the upper layer is blue and winds induced in the lower layer by upper-layer PV are also blue, with v indicated by solid and w by dashed arrows; similarly, the bottom layer is red and winds induced in the upper layer by lower-layer PV are red. See text for a physical description of the instability shown in each panel.

lower layer (layer 3) but a westward shift in the upper layer (layer 2). This is exactly the mechanism of propagation that has been discussed by multiple authors (e.g., Rao and Rajamani 1970; Raymond and Jiang 1990; Parker and Thorpe 1995). Note that the top two layers have $\overline{q}_y > 0$ and $\overline{q}^*_y > 0$ while the bottom two have $\overline{q}_y < 0$ and $\overline{q}^*_y < 0$.

Instability can be generated by four possible interactions between anomalies in different layers, and these interactions are illustrated schematically in Fig. 4. The classic dry baroclinic instability resulting from the interaction of two counterpropagating Eady edge waves is shown in Fig. 4a and occurs because each PV anomaly is associated with a nonzero circulation at all other levels as a result of the "action at a distance" property of PV inversion (e.g., Heifetz et al. 2004). The fully moist instability, in which growth arises from vertical interactions between two moist CRWs, is illustrated in Fig. 4b. In that instability, an eastward-propagating wave in the lower moist layer (layer 3) produces ascent and diabatic heating that is nonzero in the upper moist layer; this constitutes a remotely induced PV source that can amplify a westward-propagating wave in the upper moist layer if that upper-level wave has the correct relative phase. This is the instability mechanism proposed by Snyder and Lindzen (1991) and does not require any dry mean PV gradient. As in the purely dry case, the vertical interaction of these two moist CRWs can produce changes in the wave phase speeds or in their amplitudes. Mutual amplitude growth requires a phase difference of 0–π between waves in the two levels. But the waves must remain stationary relative to each other in order to have sufficient time to grow; this requires a reduction in their respective phase speeds and a phase difference of $\pi/2$–$3\pi/2$ between levels. Hence, for mutual growth and phase locking a phase shift of $\pi/2$–π is required. This phase difference is illustrated by the tilted vertical rectangles in Fig. 4, which are drawn to

emphasize the fact that vertical columns of anomalous PV must tilt upshear in order for the instability to occur. Thus, the criterion that baroclinic growth can occur only when PV anomalies tilt upshear holds for the interaction of two moist CRWs just as it did for the classic dry case.

There are two remaining interactions that can generate instability that we have not yet discussed in detail, and both involve coupling of a moist CRW with a dry CRW. The ''diabatic Rossby wave,'' as it was named by Parker and Thorpe (1995), consists of an eastward-propagating dry wave near the surface (layer 4, Fig. 4c) that interacts with a westward-propagating moist wave above the diabatic heating maximum (layer 2, Fig. 4c). When PV columns tilt upshear across these two layers, the low-level positive PV anomaly generates ascent and latent heating to its east, which in turn produces a PV sink and amplifies the negative PV anomaly in the upper layer. To be clear, the term ''diabatic Rossby wave'' and the moist quasigeostrophic propagation mechanism described by Parker and Thorpe (1995) and other authors (Rao and Rajamani 1970; Sanders 1984; Raymond and Jiang 1990) more accurately describe the zonal propagation of the moist CRW in either of our model's interior layers. Here we follow de Vries et al. (2010) and use the term to describe the instability resulting from the interaction of latent heating with low-level baroclinicity (and thus the interaction of layers 2 and 4, since the waves in layers 3 and 4 propagate in the same direction and so cannot generate instability).

Finally, we note that the interaction between a westward-propagating dry wave in the top layer and an eastward-propagating moist wave in layer 3 also generates an instability in an analogous way (Fig. 4d), which de Vries et al. (2010) called ''type C'' baroclinic growth but which we refer to as a ''tropopause intrusion'' because of the interaction of tropopause troughs with latent heating (Plant et al. 2003).

This PV view yields a few necessary conditions for baroclinic instability: (i) instability takes place only if PV (or equivalent PV) gradients take opposite signs at the respective levels (the ''home bases'') of each CRW (Charney and Stern 1962); (ii) the basic-state flow must be more positive where the PV (or equivalent PV) gradient is positive, so that the intrinsic propagation of the CRWs is opposite to the local mean wind (Fjørtoft 1950); and (iii) for mutual growth and phase locking, anomalies of PV must lean against the vertical shear of the mean flow (e.g., Fig. 4).

b. *Energetic perspective*

Another view of baroclinic instability emphasizes energy conversions (Pierrehumbert 1995) but requires the same upshear tilt of PV anomalies to obtain disturbance growth. In essence, baroclinic instability is a process by which small perturbations extract (available) potential energy from the environment. This requires a basic state with vertical shear or, alternatively, with a meridional temperature gradient. The instability process releases potential energy by reducing the tilt of the mean isentropes.

To illustrate this perspective in a moist atmosphere, we write the zonal-mean quasigeostrophic zonal momentum and moist thermodynamic equations linearized about mean flow with a westerly vertical shear (e.g., Pedlosky 1987; Yano and Emanuel 1991),

$$\overline{u}_t - f_0\overline{v}_a = -(\overline{v'u'})_y \quad \text{and} \quad \overline{b}_t + N_*^2\overline{w}_a = -(\overline{v'b'})_y, \tag{14}$$

where subscripts on geostrophic terms are omitted, but a denotes ageostrophic terms and primes denote deviations from the zonal-mean geostrophic flow. The reduced stratification $N_*^2 = (1 - \varepsilon_3)N^2$ provides a bulk representation of moist processes, consistent with convective quasi-equilibrium theories (e.g., Emanuel et al. 1994). In this view, adiabatic cooling is offset by latent heat release in ascending regions, which effectively reduces the resistance of the flow to vertical perturbations. The nondimensional parameter $0 \le \varepsilon_3 < 1$ is zero for dry atmospheres but approaches one for saturated atmospheres. Previous studies of moist baroclinic growth have used nonlinear generalizations of the second equation in (14) by allowing the effective static stability to approach zero in regions of saturated ascent while retaining its dry value in regions of subsidence (e.g., Emanuel et al. 1987). We use the simpler and crude constant value of N_* for purposes of discussion.

The evolution of the total energy of the mean flow $\overline{E} = 0.5(\overline{u}^2 + \overline{b}^2/N_*^2)$, which is the sum of the kinetic and available potential energy, can be achieved by multiplying the first equation in (14) by $\overline{u}$, the second equation in (14) by $\overline{b}/N_*^2$, and adding the two. Integration over a closed domain $\mathscr{D}$ and integration by parts yields (e.g., Pedlosky 1987)

$$\int_{\mathscr{D}} \overline{E}_t\, dx = \int_{\mathscr{D}} \left[\overline{u}_y(\overline{v'u'}) + \frac{1}{N_*^2}\overline{b}_y(\overline{v'b'}) \right] dx. \tag{15}$$

In the real atmosphere, (15) would include a term associated with moisture anomalies, but in our conceptual model moisture is horizontally invariant (as in previous analytical models of moist baroclinic instability) and its effects are represented entirely in terms of a reduced static stability. Assuming quasi geostrophy and thermal wind balance, $(u, v, b) = (-\psi_y, \psi_x, f_0\psi_z)$ and $\overline{b}_y = -f_0\overline{u}_z$, which allows the integrand on the right-hand side

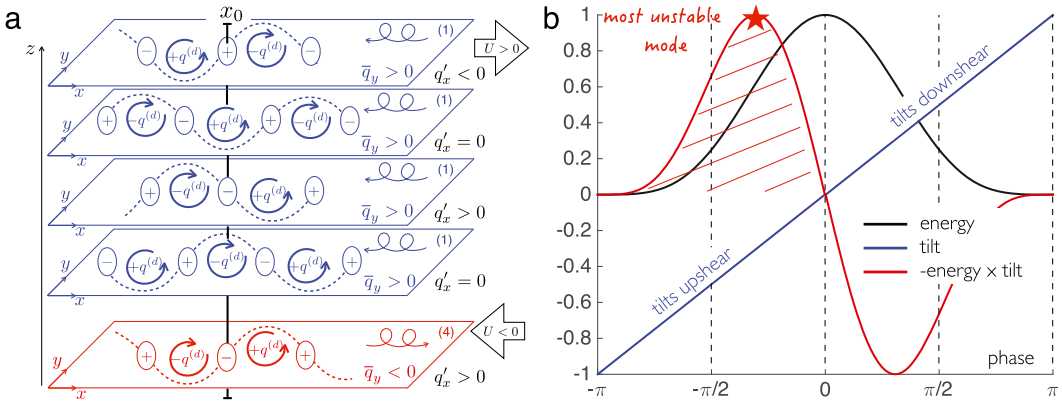

FIG. 5. Illustration of the energy perspective on baroclinic growth. (a) The dry baroclinic scenario of Fig. 4a, with symbols as described in Fig. 3. The bottom layer (4; red) is stationary about x_0 while the top layer (1; blue) moves eastward relative to the bottom wave as one moves down in the panel. (b) The perturbation energy (black line), phase tilt (blue line), and the rate of growth of disturbance energy (red line), all normalized by their maximum values. The sign of the zonal gradient in q' at x_0 is marked on the right side of each layer. Perturbation energy is taken to be simply $\overline{q_x'^2}$ and the growth rate of this energy is the product of the energy and tilt, as in (16). The hatched area marks phases where disturbance growth occurs and the red star marks the maximum of this rate, which occurs for the most unstable mode in the long time limit.

of (15) to be written, using the implicit function theory,[5] as

$$\overline{u}_y(\overline{v'u'}) = -\overline{u}_y(\overline{\psi_x'\psi_y'}) = \overline{u}_y\left(\overline{\psi_x'^2\frac{dx}{dy}\Big|_{\psi'}}\right) \quad \text{and}$$

$$\frac{1}{N_*^2}\overline{b}_y(\overline{v'b'}) = -\frac{f_0^2}{N_*^2}\overline{u}_z(\overline{\psi_x'\psi_z'}) = \frac{f_0^2}{N_*^2}\overline{u}_z\left(\overline{\psi_x'^2\frac{dx}{dz}\Big|_{\psi'}}\right). \qquad (16)$$

Disturbance growth is achieved if perturbations grow in time, which can occur only if the energy of the mean flow decreases,

$$\int_{\mathscr{D}} \overline{E}_t\, dx < 0. \qquad (17)$$

It is then clear from (16) that perturbations (e.g., isolines of constant ψ') must lean (i.e., slope) against the meridional or vertical shear. While the former is a requirement for barotropic growth, the latter is a requirement for moist baroclinic growth. Since q anomalies will have the same tilt as ψ anomalies, this confirms that PV anomalies must tilt against the shear for growth to occur. No assumption of instability has been made here, and (17) could hold for some finite time during which transient growth of a stable disturbance occurs, as discussed by Farrell (1982) for stable dry baroclinic growth. Here the generalization to moist disturbances has been achieved by the somewhat crude transformation $N \to N_*$ in (14).

The connection to the PV framework discussed above can be understood by considering how disturbance energy changes as two CRWs propagate relative to each other. We illustrate this using the dry baroclinic instability case of Fig. 4a, but this applies equally to interactions involving moist CRWs by virtue of the fact that they can be represented as PV anomalies. Consider the case in which the top CRW in layer 1 moves eastward relative to the bottom CRW in layer 4; that is, the eastward mean flow at layer 1 is faster than the intrinsic westward phase speed at that level. According to (16), the rate of change of disturbance energy is proportional to the product of $\psi_x'^2$ and the vertical tilt in ψ', which are respectively proportional to $q_x'^2$ and the tilt in q'. Here we represent the tilt using the phase ϕ, so that the two CRWs are in phase for $\phi = 0$, and we assume q' is sinusoidal in x.

The vertically integrated wave energy $E' \propto \overline{q_x'^2}$ is maximum when q' anomalies are in phase ($\phi = 0$) and minimum when q' anomalies are out of phase ($\phi = -\pi$). As the top CRW moves eastward its phase ϕ changes (Fig. 5a) together with the vertically integrated wave energy (Fig. 5b). Disturbance amplification requires energy transfer from the mean flow to the perturbation, which occurs when q' anomalies tilt upshear ($-\pi < \phi < 0$ in our schematic). This is described by the second equation in (16), the right-hand side of which is the negative of the rate at which energy is transferred from the mean flow to the disturbance. Positive growth of disturbance energy in this example is indicated schematically by the hatched red area in Fig. 5b. It is largest for upshear tilts somewhat larger than $-\pi/2$ (marked by the red star), which would be

[5] That is, along lines of constant ψ' in the x–y plane, $\psi'[x, y(x)]$ is constant. Thus, $d\psi' = \partial\psi'/\partial x + (\partial\psi'/\partial y)(dy/\partial x) = 0$ and $\partial\psi'/\partial x = -(\partial\psi'/\partial y)(dy/dx)$. Similar analysis can be applied to obtain the second equation in (16).

TABLE 2. Details of the three track datasets analyzed here. All disturbances examined formed during June–September.

	Low pressure system		
	MDs	Hurricanes	DRWs
Years	1979–2012	1996–2012	2006–10
Number of storms	117	103	110
Tracking algorithm	Yale dataset	NHC dataset	ETH dataset
Domain	Bay of Bengal (10°–27°N, 75°–95°E)	North Atlantic (5°–40°N, 95°W–15°E)	North Atlantic (28°–54°N, 105°W–5°E)

associated with the most unstable linear normal mode in a classic linear stability analysis. This is consistent with the tilts required to achieve amplification and phase locking of the two CRWs, as discussed above.

This energy perspective can also help in understanding transient growth of stable disturbances. The derivation of (17) assumed neither instability nor the existence of linear normal modes, and it could describe the time evolution of flow that is stable or in which there was not enough time for the most linearly unstable mode to grow to a dominant amplitude. In such a case, the phase in Fig. 5b could be assumed to increase with time from $\phi = -\pi$ as the top CRW propagates eastward. Transient, stable amplification would occur while the PV anomalies tilt upshear, but the disturbance would reach a peak energy at $\phi = 0$ and would then decay. Thus, even in a stable system, PV anomalies must lean against the shear to produce transient nonmodal moist baroclinic growth.

3. Data and methods

We analyze three different types of low pressure systems: MDs, hurricanes, and DRWs. For all three categories, we limit our attention to storms that form during summer (June–September) in the Northern Hemisphere. Our analyses are based on the latest global atmospheric reanalysis produced by the European Centre for Medium-Range Weather Forecasts (ERA-Interim; Dee et al. 2011). This data product spans from 1979, the start of the satellite era, to the present and has horizontal resolution of roughly 0.7° × 0.7°, 60 vertical levels, and temporal resolution of 6 h.

For MDs, we use the global track dataset developed by Hurley and Boos (2015) but only analyze storms forming in the main genesis region for Indian monsoon low pressure systems—the Bay of Bengal (10°–27°N, 75°–95°E). This yields 117 storms that form during 1979–2012 (Table 2). Hurley and Boos (2015) compiled this track dataset using an automated tracking algorithm to identify and follow paths of 850-hPa relative vorticity maxima, then classified the disturbances in ways consistent with traditional definitions of MDs used by the India Meteorological Department (e.g., Mooley and Shukla 1987; Sikka 2006; Ajayamohan et al. 2010). In particular, MDs were required to have a sea level pressure minimum of 4–10 hPa below that of surrounding regions and also to have a surface wind speed maximum between 8.5 and 13.5 m s^{-1}. These intensity criteria were required to be satisfied within 500 km of the 850-hPa vorticity maximum and to occur simultaneously during at least one 6-h period along the vortex track.

North Atlantic hurricane tracks are taken from the revised Atlantic hurricane best-track data that span from 1851 to 2013 (HURDAT2; Landsea et al. 2004; Landsea and Franklin 2013). This dataset is the official poststorm assessment and is maintained by the National Hurricane Center. As is standard, tropical cyclones are classified as hurricanes if their maximum sustained surface wind speed exceeds 32 m s^{-1} at least once during their lifetime. The ensemble of North Atlantic hurricanes presented here consists of 103 storms that form over 5°–40°N, 95°W–15°E during 1996–2012 (Table 2).

Tracks of DRWs are drawn from a dataset compiled by Boettcher and Wernli (2013), and here we examine storms from this dataset that formed over the North Atlantic (28°–54°N, 105°W–5°E). This provides 110 DRWs that form during 2006–12 (Table 2). Boettcher and Wernli (2013) based their identification of DRWs on multiple criteria, but some of the most salient are the existence of enhanced low-level PV, substantial baroclinicity, fast propagation, sufficient moisture, and weak upper-level forcing. We refer the reader to Boettcher and Wernli (2013) for more details but emphasize that this constitutes a set of midlatitude baroclinic storms with abundant precipitating convection—disturbances in which moist baroclinic instability is thought to play an essential role.

Storm-centered composite means are created by averaging fields along the storm track relative to the vortex center, as provided by the track datasets listed above. Any extrapolated ERA-Interim data that exist at pressures higher than that of the surface were omitted from the analysis. To compare the evolution of storms with different lifetimes, we use two approaches. In one approach we examine time averages over the first, middle,

TABLE 3. Ensemble-mean properties of MDs, hurricanes, and DRWs during boreal summer.

	Low pressure system		
	MDs	Hurricanes	DRWs
Lifetime (days)	10 ± 4	11 ± 5	3 ± 1
Absolute propagation speed ($m\,s^{-1}$)	5 ± 1	7 ± 2	5 ± 3
Core temperature	Warm over cold	Warm	Warm
Ambient wind shear	Strong negative (easterly)	Weakly positive (westerly)	Positive (westerly)
Ambient temperature gradient	Positive	Weak	Negative
Low-level baroclinicity	Weak	Weak	Strong
Upper-level baroclinicity	Strong	Weak	Weak
Low-level moisture anomaly	Large	Very large	Very large

and last thirds of each storm's lifetime. In the second approach we interpolate time series of each variable, in the storm-centered coordinate system, to a 10-day period. In both approaches we append 2 days of data to the beginning of the time series consisting of uninterpolated averages of fields on the 2 days prior to genesis, relative to the location of the storm center on the genesis day; this was done to obtain an estimate of the atmospheric state immediately before each storm was detected in the reanalysis. We similarly append 2 days to the end of the time series consisting of uninterpolated averages 2 days after the end of the storm, relative to the storm center on the last day of its track.

To calculate anomalies relative to the background state, it is necessary to define a proper background state. But defining such a state is not straightforward in an environment with abundant vortex activity because the vortices project strongly onto the mean state. For example, synoptic-scale low pressure systems produce over half the precipitation that falls over continental India during summer, so these low pressure systems are expected to strongly influence the climatological-mean diabatic heating and PV. The genesis location of Indian MDs and, more generally, low pressure systems is highly localized over the northern Bay of Bengal, so subtracting a simple climatological time mean would amount to subtracting at least some of the structure of a mean low pressure system. Here we define the background state as an average over the period from 3 to 5 days before the detection of a low pressure system by the relevant tracking algorithm (i.e., 3–5 days before genesis). Given the frequencies, lifetimes, and propagation speeds of the storms examined here (Tables 2 and 3), this 5-day period is substantially shorter than the average interstorm period. Deviation fields are defined as the difference between a total variable sampled in the storm-centered reference frame and the same variable sampled at the same location from this background state. Since our ensembles contain roughly 100 storms each, the total number of days that is used for creating average background states is the product of 300 and the average storm lifetime (e.g., 3000 days for MDs).

4. Results

a. The baroclinic environment

To gain insight into the mechanisms responsible for MD growth, we compare the evolution of MDs with that of hurricanes and DRWs. As is well known, latent heat released by precipitating convection plays a central role in the energy transfers within hurricanes, but they are more fundamentally driven by the thermodynamic disequilibrium between the ocean surface and the overlying atmosphere [see review by Emanuel (1991)]. After formation, hurricanes propagate to the northwest at an average speed of about $7\,m\,s^{-1}$ and have an average life span of about 11 days (Fig. 1 and Table 3). They evolve in environments with relatively weak vertical shear and warm temperatures, until the latter part of their lifetimes when they propagate into the cold extratropics (Fig. 6). In contrast, DRWs are a special category of extratropical cyclones in which precipitating convection is thought to strongly modify the process by which the available potential energy stored in the extratropical meridional temperature gradient is converted to storm kinetic energy (Moore and Montgomery 2004; Boettcher and Wernli 2011, 2013). DRWs propagate as a result of continuous diabatic regeneration of low-level positive PV anomalies downshear of their current vortex center. After formation, they propagate to the northeast at an average speed of about $5\,m\,s^{-1}$ and have an average life span of about 3 days (Fig. 1 and Table 3). DRWs evolve in an environment of strong westerly vertical shear and thus propagate from warmer toward colder regions (Fig. 6).

MDs evolve in an environment that has substantially stronger shear than that of hurricanes; although this shear is easterly instead of westerly, it is nearly comparable in amplitude to that in the environment of DRWs (Fig. 6a). Because the Coriolis parameter is only about

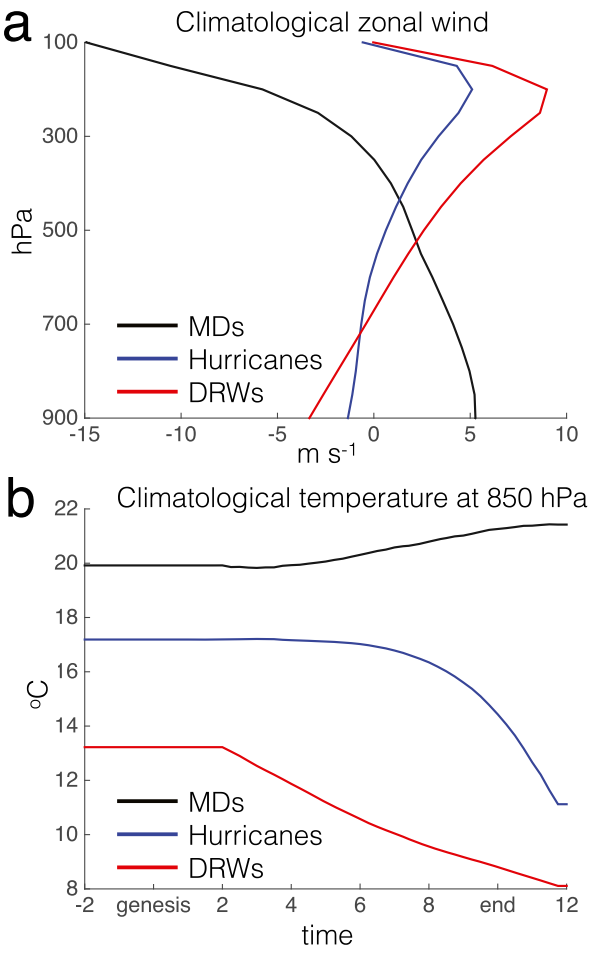

FIG. 6. (a) Climatological vertical profile of zonal wind and (b) time series of 850-hPa temperature over storm lifetimes for each ensemble of storms. The climatology is defined as the background state created by averaging 3–5 days prior to genesis and the temperature time series were obtained by interpolating each storm to a 10-day period, as described in section 3.

half as large for a typical MD as it is for the DRWs studied here, the magnitude of the meridional temperature gradient and thus the available potential energy in the environment of MDs is expected to be weaker. The MD environment also has the same sign of vertical shear in the lower troposphere, the upper troposphere, and the lower stratosphere, in contrast to that of hurricanes and DRWs where the shear changes sign at about 200 hPa. Nevertheless, there is still some available potential energy from which MDs might draw during their amplification. The propagation of MDs is also to the northwest, like hurricanes, but in the monsoon environment this involves movement into warmer regions. The fact that the environment of hurricanes and DRWs has a negative meridional temperature gradient ($\overline{T}_y < 0$) while that of MDs has a positive gradient ($\overline{T}_y > 0$) has implications for the solution of the omega equation and the location of ascent/descent in a given vortex [see (7), (9), and Fig. 2]. Indeed, if one accounts for the reversal in sign of the environmental vertical shear, the diabatic propagation of DRWs is similar to that originally thought to govern the movement of Indian MDs [see discussion in Boos et al. (2015)]. However, Indian MDs have been shown to propagate primarily by horizontal adiabatic advection of PV, with strong resemblance to the mechanisms responsible for the movement of tropical cyclones (Boos et al. 2015, 2016). Another difference between the three types of storms is the vertical temperature structure of their inner vortex (shown in Fig. 8). While MDs have a clear cold core in the lower troposphere that lies beneath a warm middle and upper troposphere (e.g., Godbole 1977), hurricanes and DRWs have a warm-core structure (Table 3).

McTaggart-Cowan et al. (2008, 2013) developed a dynamically based categorization scheme for tropical cyclones that we will now use to compare the development of MDs, hurricanes, and DRWs. This scheme is based on the upper-level quasigeostrophic forcing for ascent (called the "Q metric") and the low-level baroclinicity (called the "Th metric"). The Q metric is computed here as the 200–400-hPa, 29° × 29° storm-centered average of the quasigeostrophic forcing for ascent only (i.e., the **Q**-vector convergence multiplied by a Heaviside function before averaging), while the Th metric is computed as the difference between the 90th and 10th percentiles of the 700–1000-hPa geopotential height within the same 29° × 29° box. Figure 7 shows the Q and Th metrics, plotted on the horizontal and vertical axes, respectively, 1 day prior to storm genesis (analysis of the 2 days prior to genesis yields essentially the same result and is not shown). It can be seen that DRWs develop in a much more baroclinic environment than MDs or hurricanes. This is consistent with our previous statement that, although the magnitude of the vertical wind shear is similar in the environment of MDs and DRWs, one would expect the available potential energy to be weaker in the environment of MDs given their lower latitude. It is striking to notice the similar environment in which both MDs and hurricanes develop, at least in this Q–Th space. Thus, while baroclinic processes may play some role in the genesis of hurricanes and MDs, they are substantially weaker for those two types of storms than for DRWs.

b. *Potential vorticity structure*

We now examine the PV of our three ensembles of storms with the goal of assessing which disturbances have PV structures that tilt against the shear, as one would expect for disturbances growing through

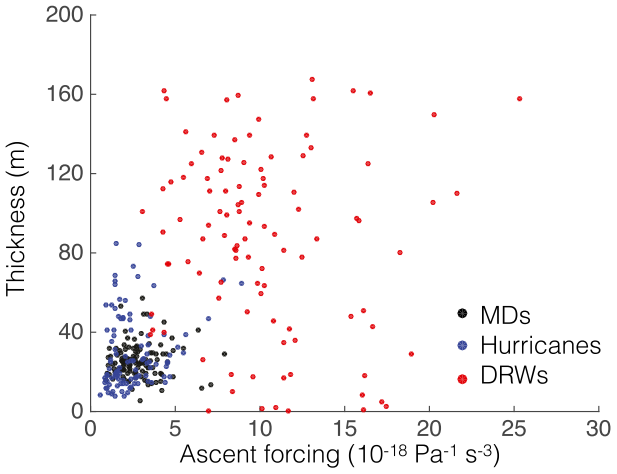

FIG. 7. Scatterplots of the Q and Th metrics 1 day prior to storm genesis, with one point plotted for each storm. The Q metric provides a measure of the upper-tropospheric quasigeostrophic forcing for ascent and Th indicates the low-level baroclinicity, as described in the text.

baroclinic instability. Figure 8 shows the ensemble-mean anomalous PV during the 2 days prior to storm genesis and during each third of the life cycle for each category of storm. Although we do not average only over times during which growth occurs, the average MD does grow during nearly all of the first third of the life cycle and decays during the last third (not shown). The shear direction is noted for reference by a vector at the bottom left of each panel. As discussed above (e.g., Fig. 6a), hurricanes and DRWs typically grow in environments with westerly vertical shear ($\overline{u}_z > 0$) while MDs grow in easterly shear. Thus, to satisfy our diagnostic criterion for baroclinic growth, the deviated PV must tilt westward with height (toward negative longitudes) for hurricanes and DRWs but must tilt eastward with height for MDs.

Figure 8 (right column) shows clearly that, in the ensemble-mean DRW, positive upper-tropospheric PV anomalies are positioned upshear of strong low-level PV anomalies during all three phases of the life cycle and on the day prior to genesis. For example, on day −1 positive PV anomalies at 500 and 200 hPa lie, respectively, about 5° and more than 12° of longitude upshear of a positive PV anomaly at 900 hPa (the 200-hPa anomaly is outside the domain shown in Fig. 8 on day −1). During the main three life-cycle phases of DRWs, a strong positive upper-tropospheric PV anomaly is positioned about 10° upshear of a nearly vertical column of positive lower-tropospheric PV. In contrast, the ensemble-mean PV perturbation for hurricanes (Fig. 8, middle column) extends from the surface to about 300 hPa in a vertical column that exhibits little to no tilt during the 2 days prior to genesis and during the first two-thirds of the life cycle. A strong 200-hPa cyclonic PV anomaly does appear upshear of this vertical column during the last one-third of the life cycle, which we speculate may be part of an extratropical transition process. The existence of an upper-level negative PV anomaly downshear of a lower-level positive anomaly is equivalent to an upshear tilt and is observed throughout the life cycle of DRWs; a similar though somewhat weaker feature is seen for hurricanes and is, again, most prominent during the last third of the composite-mean life cycle. Thus, DRWs exhibit a strong tilt of their PV against the environmental vertical shear while hurricanes exhibit little evidence for a tilt against the shear during the growth phase of their life cycle, as expected for these two classes of storms. Recall that PV increases with the Laplacian of the horizontal streamfunction, so tilts in the wind and geopotential height fields can also be inferred from these plots.

In contrast, the ensemble-mean MD exhibits no upshear tilt and, in fact, has PV anomalies that tilt downshear throughout most of the life cycle (Fig. 8, left column). The initial cyclonic PV anomaly that appears during the 2 days prior to genesis is confined almost entirely below 400 hPa and tilts downshear across nearly 24° of longitude. The PV column becomes more intense and upright during the first third of the life cycle but still exhibits a slight downshear tilt, with the maximum PV at 500 hPa lying about 1° downshear of the 750-hPa maximum, and the maximum PV at 300-hPa lying even farther downshear. Unlike hurricanes and DRWs, there is no negative PV anomaly at upper levels. Note that during the first third of their life span both MDs and hurricanes exhibit a warm-over-cold structure, while DRWs evolve with a more classic baroclinic structure.

We further examine the evolution of near-surface temperature anomalies during storm development because baroclinic instability can arise from the interaction between interior PV anomalies and surface temperature anomalies (e.g., Vallis 2006). Bretherton (1966) showed that when inverting PV, a temperature anomaly on a boundary produces an interior state equivalent to that achieved by inverting the same PV field with homogeneous boundary conditions and a δ function of PV immediately next to the boundary. Since temperature boundary conditions were not considered in the conceptual model used to derive our necessary criterion of PV anomalies tilting against the shear, we now incorporate them by treating lower boundary potential temperature anomalies as equivalent δ functions of PV. In other words, we ask whether interior cyclonic PV anomalies lie upshear of near-surface warm anomalies. Because these storms develop in different geographic

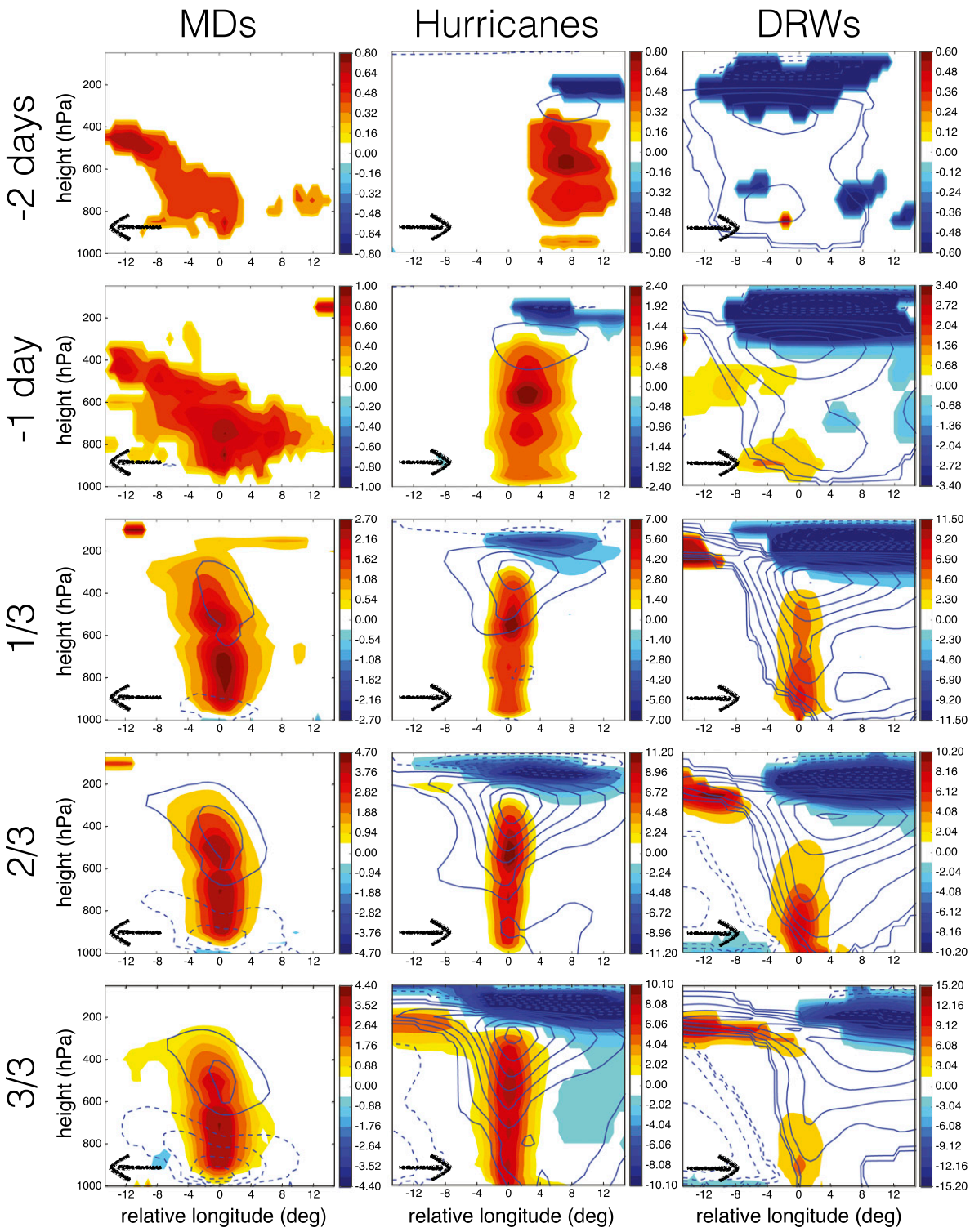

FIG. 8. Ensemble-mean, storm-centered anomalous Ertel's PV (color shading; PVU) and temperature (contours; K) (top two rows) for 2 days and 1 day before genesis and (bottom three rows) during the first third, second third, and last third of storm lifetime. Only statistically significant (at the 1% level) fields are shown. Note the different scale for PV used in each panel. The temperature contour interval is 0.5 K with negative contours dashed and the zero contour omitted. The arrow at the bottom left of each panel shows the direction of the climatological vertical shear (i.e., the 200- minus 850-hPa zonal wind).

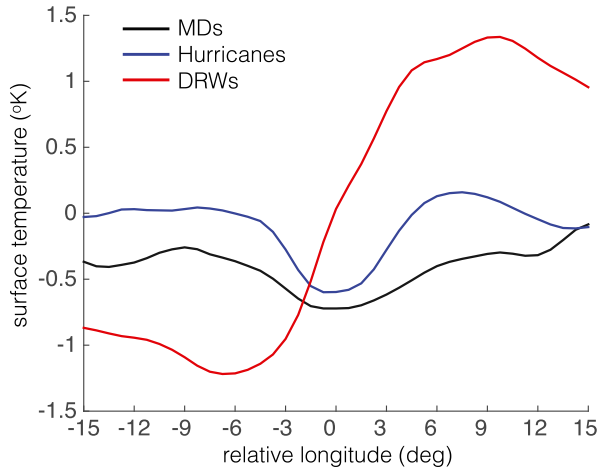

FIG. 9. Zonal structure of storm-centered ensemble-mean near-surface temperature anomalies (on ERA-Interim model level 54 out of 60, $\sim\sigma = 0.95$) during the first third of the storm life cycle.

regions with varying surface pressures, it is possible that the pressure-level composites shown in Fig. 8 do not properly represent near-surface temperature anomalies. So we also plot in Fig. 9 near-surface temperature anomalies during the first third of the life cycle in terrain-following coordinates ($\sim\sigma = 0.95$, model level 54 out of 60). This confirms, consistent with the temperature contours in Fig. 8, that there is a clear zonal temperature gradient that extends across DRWs as in a classic baroclinic wave (the cold anomalies on the west side of the DRWs during the first third of their life time in Fig. 8 are not statistically significant) and that there is a low-level cold anomaly at the center of hurricanes during their development phase. MDs also have a cold core at low levels, and there is no evidence for a near-surface warm anomaly downshear of the interior positive PV. Thus, there is no evidence that surface temperature anomalies interact with interior PV anomalies in a way that would foster baroclinic growth in MDs. A somewhat tangential novel finding here, though, is that the low-level cold anomaly in MDs increases strongly in amplitude throughout the ensemble-mean life cycle (Fig. 8).

To be more quantitative with our "tilting against the shear" diagnostic, we devise a metric that quantifies the amount of tilt present in the PV field and examine how this metric is distributed within each ensemble and over time. This addresses the possibility that the ensemble-mean PV distributions discussed above disguise structures that would indicate baroclinic instability in individual storms. We define this metric as the longitudinal difference between the "center of mass" of the upper- (200–500 hPa) and lower- (600–900 hPa) level positive PV anomalies, multiplied by the sign of the climatological vertical wind shear, and call this the tilt-against-the-shear (TATS) metric,

$$\mathrm{TATS} = -\Delta\tilde{\lambda}\,\mathrm{sgn}(\Delta\overline{u}), \quad \text{where} \quad \tilde{\lambda} \equiv \frac{\int q'_+\lambda\, d\lambda\, dp}{\int q'_+\, d\lambda\, dp}. \tag{18}$$

Here λ is longitude, q'_+ is the storm-centered positive PV anomaly $q'_+ = q'\mathscr{H}(q')$ with $\mathscr{H}$ the Heaviside function, and $\overline{u}$ is the basic-state zonal wind. The Δ operator takes a difference between the 200–500- and 600–900-hPa layers, where the mean zonal wind $\overline{u}$ is also averaged over these two layers before the difference is applied. Positive TATS values thus indicate that perturbations tilt against the shear (needed for baroclinic instability), and negative values indicate downshear tilts. We found that many storms have weak upper-level PV anomalies during parts of their lifetimes, so we also require that the upper-level (200–500 hPa) anomaly have a minimum amplitude given by $\int q'_+\, d\lambda\, dp > 0.3\,\mathrm{PVU} \times 4^\circ \times 200\,\mathrm{hPa}$, where $1\,\mathrm{PVU} = 10^{-6}\,\mathrm{m^2\,K\,s^{-1}\,kg^{-1}}$.

Estimates of the probability density functions (PDFs) of the TATS metric, obtained via a kernel density estimate, confirm that the tilts seen in the ensemble-mean structures are generally characteristic of the individual storms within each ensemble (Fig. 10). For example, the PDFs for DRWs are strongly skewed toward upshear tilts during each of the three main phases of the life cycle: at least two-thirds of DRWs tilt upshear in each phase. The downshear tilts that do occur for DRWs during the first third of the life cycle are quite weak, and the mode of the distribution has a TATS value ranging from 3° to 8° throughout the life cycle. In contrast, hurricanes and MDs have comparatively narrow PDFs that peak at zero during the growth phase, indicating that nearly all storms have an upright structure with little detectable tilt. It is only in the latter stages of the life cycle that many hurricanes develop upshear tilts, consistent with the ensemble-mean behavior shown in Fig. 8. The PDFs for MDs are skewed slightly toward downshear tilts (negative TATS and negative skewness) during the main three phases of the life cycle, which shows that most MDs cannot be growing by dry or moist baroclinic instability. Qualitatively similar results are obtained when the TATS measure is defined using the maximum PV anomaly in each of the two layers instead of the center of mass of the PV anomaly (not shown).

Although the PDFs of our TATS metric are centered on zero for MDs, they are wide enough that it seems reasonable to wonder if some fraction of MDs is growing by baroclinic instability. We investigate this possibility

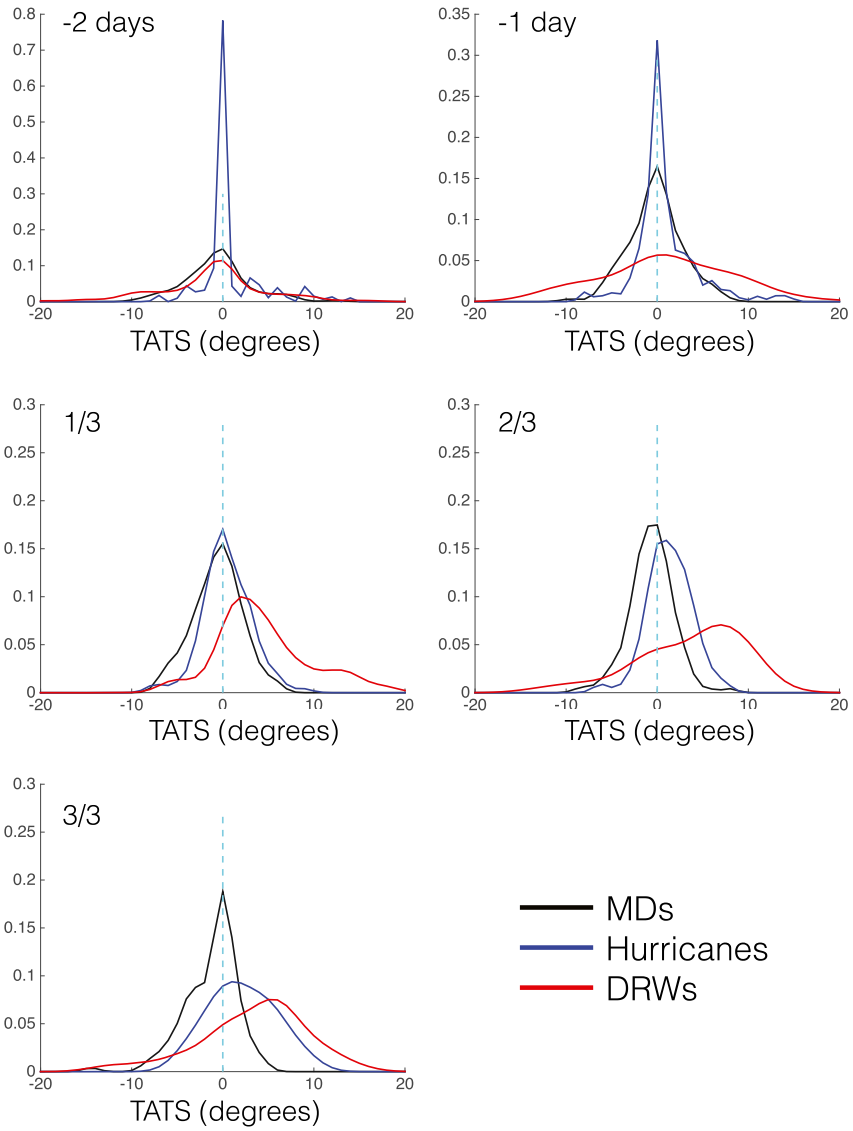

FIG. 10. Estimated probability density functions of the TATS metric, as defined in (18), in each ensemble (top) 2 days and 1 day prior to genesis and (middle),(bottom) during each third of storm life cycle. Positive values indicate vertical tilts against the shear.

by examining the PV structures of individual storms that have positive TATS during the first third of their life cycles. We choose two MDs with TATS values of about 3.5°. Inspection of the anomalous PV confirms that there is indeed an upper-level positive PV anomaly upshear of the lower-level anomaly during the growth phase, especially in case 1 (see the positive PV at 12° relative longitude and 400 hPa in Fig. 11, left column), but the PV field is fairly noisy and lacks a clear and coherent structure that tilts upshear. Given that these upshear, upper-level PV anomalies are only a few hundred kilometers in horizontal scale, it seems unlikely that they would strongly interact with the low-level anomalies: the Rossby penetration depth of a 500-km-wide PV anomaly is only about 2 km in the South Asian monsoon region [see discussion in Boos et al. (2015)]. Furthermore, any upshear tilt, as indicated by the TATS metric, seems to be highly transient in these two as well as other cases of MDs. In contrast, two cases of DRWs with TATS values of 5.0° and 3.5° exhibit similar upshear tilts to those seen in the ensemble means (Fig. 12). The upshear tilts in these DRW cases are also highly persistent in time as the disturbances develop and even as they decay in the last part of the life cycle. The early stages of DRW

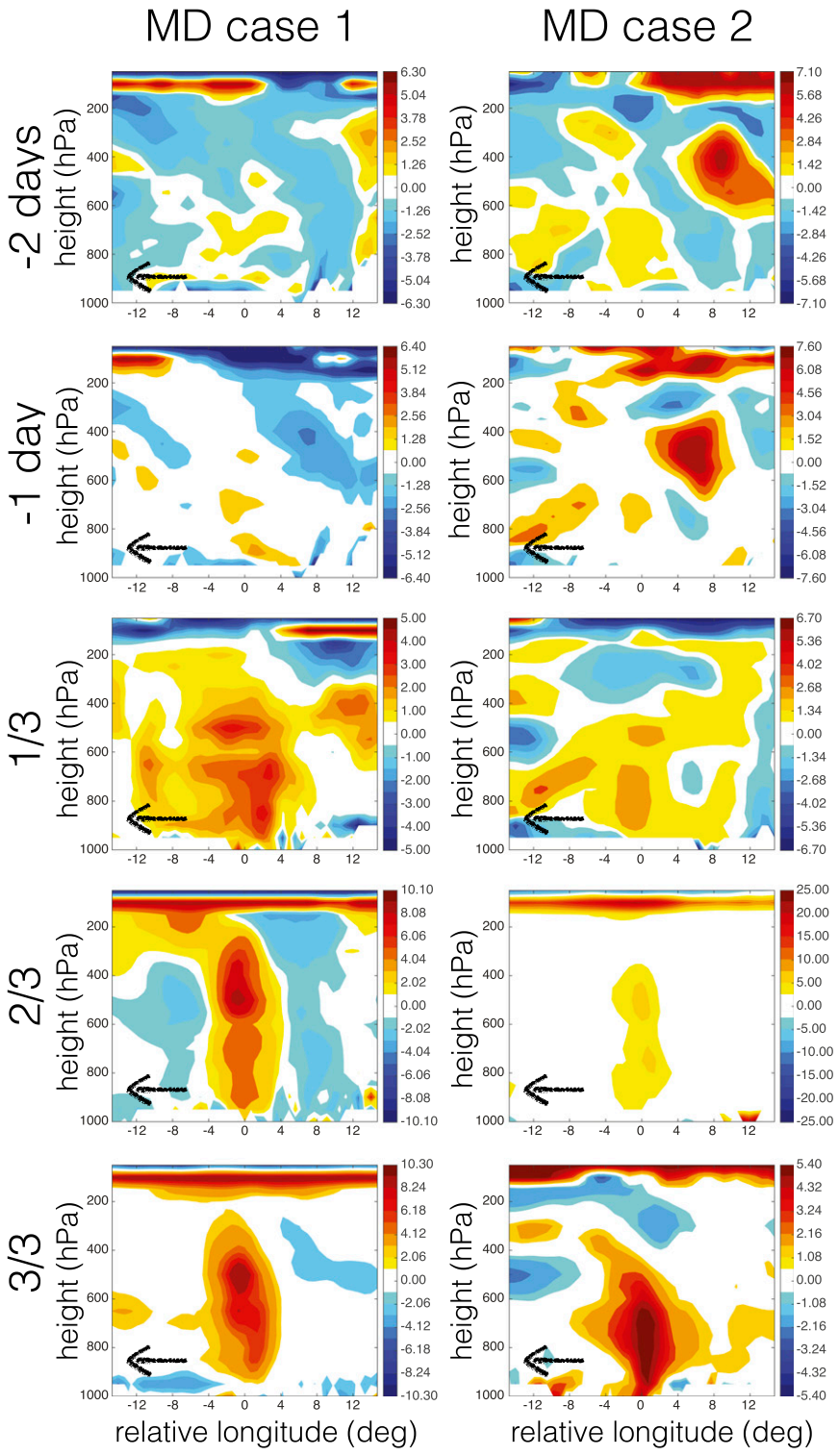

FIG. 11. As in Fig. 8, but for two individual MDs that developed with positive TATS values during the first third of their lifetimes.

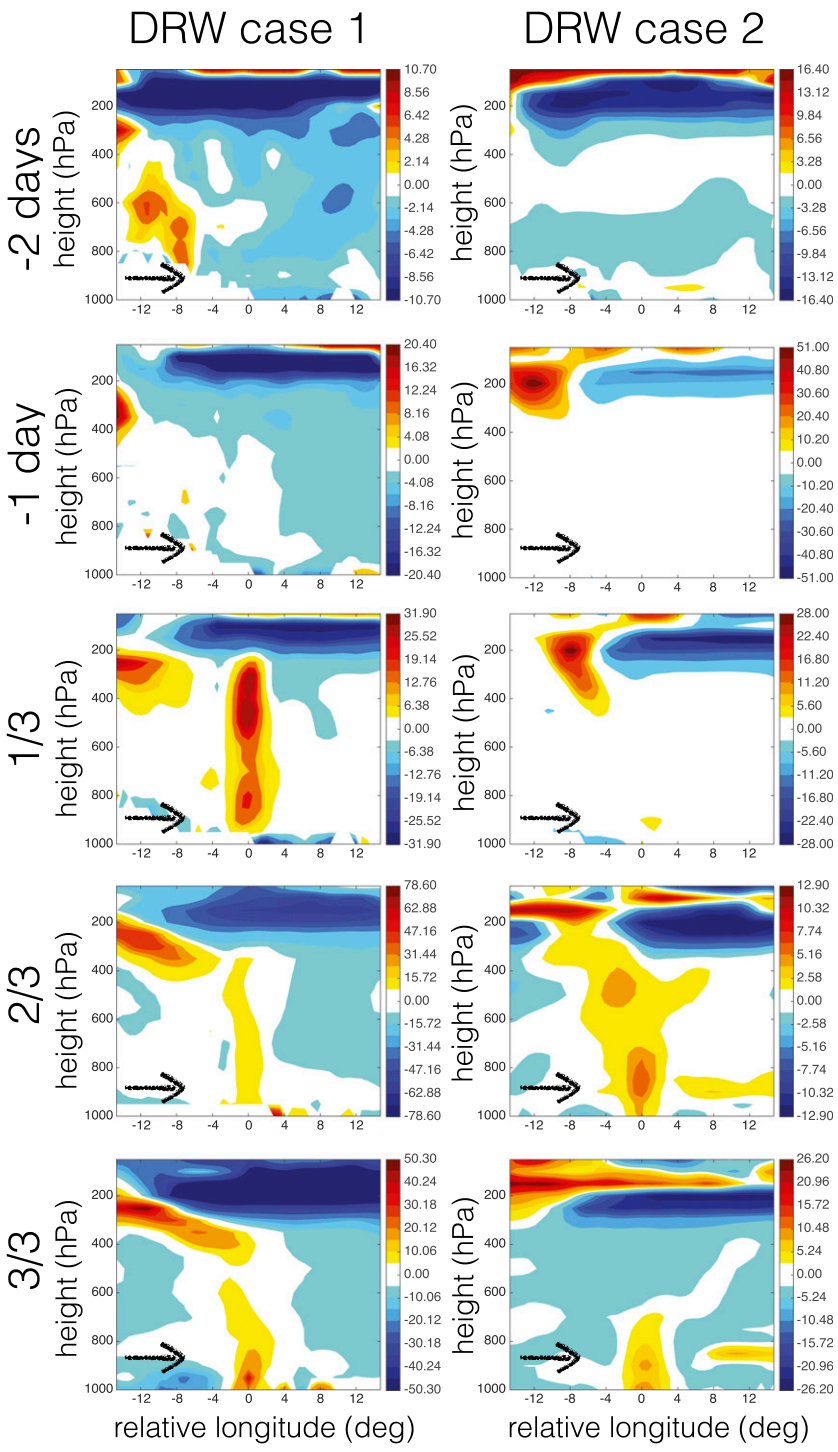

FIG. 12. As in Fig. 8, but for two DRWs that developed with positive TATS values during the first third of their lifetimes.

case 2 are strongly suggestive of a tropopause intrusion type of growth, as the upper-level anomaly is quite strong (about 5 PVU) and there is no discernible low-level PV anomaly until later in that storm's life cycle.

5. Summary and discussion

Monsoon depressions are synoptic-scale low-pressure systems that develop during local summer in monsoon

climates. Although they have been studied for over five decades, little is known about the physical mechanisms responsible for the genesis and intensification of these heavily precipitating storms. The existing theoretical work largely attributes the growth of MDs to moist baroclinic instability, although analyses have been limited to highly idealized linear models and few detailed comparisons with observations have been conducted. Here we examined whether moist baroclinic instability is responsible for the growth of MDs, comparing their dynamical structure with that of two other prototypical classes of storms: hurricanes and diabatic Rossby waves.

Motivated by the fact that mechanisms for moist baroclinic instability have been presented by multiple previous studies with unclear commonalities, we began by presenting a conceptual model that captures the multiple types of interaction that can lead to instability in a moist, baroclinic basic state. This PV framework is essentially that examined by de Vries et al. (2010), but we focused on reviewing the physical mechanisms involved in each type of instability and deriving a simple criterion that can be used to identify baroclinic instability in observations. In particular, we showed that the upshear tilt of PV anomalies needed for classic dry baroclinic growth is also necessary for moist baroclinic instability, even though the diabatic heating of moist convection supplies PV sources and sinks that are not part of traditional models for dry baroclinic growth. Although one might obtain this result by assuming that precipitating convection simply reduces the effective static stability in the classic dry problem, explicit consideration of the diabatic sources and sinks of PV provides a more detailed mechanistic view of the multiple types of moist instability and a better connection with the literature that views baroclinic instability as the interaction of counterpropagating Rossby waves. We hope that clear identification of this necessary criterion—the upshear vertical tilt of anomalous PV—will aid in future observational studies of precipitating, synoptic-scale systems other than MDs.

Using reanalysis data, we showed that DRWs clearly exhibit upshear tilts during their spinup period. This was shown in ensemble-mean, storm-centered composites and, through development of a metric that quantifies the tilt of anomalous PV, was also shown to apply across most of the distribution of individual DRWs. The upshear tilt actually seemed to persist throughout the mature stages of the DRW life cycle. Hurricanes exhibited negligible tilt during their development but did tilt upshear late in their lifetime, which we speculate is due to interaction with midlatitude baroclinic waves in extratropical transitions.

We found no evidence that moist baroclinic instability contributes to the genesis or growth of MDs. The ensemble-mean MD tilted slightly downshear, rather than upshear, and the distribution of individual MD tilts was skewed in favor of downshear tilts. Examination of some individual MDs that did exhibit upshear tilts, as measured by our TATS metric, revealed that these tilts were associated with upper-level PV anomalies that were weak and incoherent compared to the well-defined structures seen in DRWs. In other words, one would expect ''noise'' in the PV field to produce some negative TATS values even for storms that have coherent upright structures, and our case studies of MDs with upshear tilts were not clearly distinguishable from such a scenario. There was also no evidence that surface temperature anomalies contribute to moist baroclinic growth, which we demonstrated (e.g., Fig. 9) by considering their conceptual equivalence with boundary PV anomalies (Bretherton 1966).

The possibility that horizontal moisture advection plays a role in the dynamics of MDs was not examined here and does not seem to have been considered in previous studies. As mentioned in our review of existing analytical models of moist baroclinic instability, those models do not include a prognostic moisture equation that could represent horizontal moisture advection. However, idealized numerical simulations of DRWs have shown that meridional advection of moisture downshear of the vortex center moistens the lower troposphere during the genesis of these storms, ''preconditioning'' the atmosphere so that the quasigeostrophic ascent can produce precipitation and generate PV (Moore et al. 2013). In an entirely separate line of theory, Sobel et al. (2001) showed how vortices embedded in a meridional moisture gradient could propagate zonally by advecting moisture; in that system moisture controls convective heating and ascent is determined diagnostically from the heating via a weak temperature gradient approximation. This constitutes a complementary limit to that considered in the existing literature on MDs and moist baroclinic instability, with ascent and diabatic heating set by a prognostic moisture field instead of by dry adiabatic dynamics. Determining whether that limit is relevant to MDs and DRWs seems a fruitful avenue for future study.

The mechanism responsible for MD intensification thus remains unknown. Yet ruling out baroclinic instability is a novel and important accomplishment, since it seemed to be the most commonly accepted theory for MD growth (e.g., Shukla 1978; Mak 1983; Krishnakumar et al. 1992; Parija and Dash 1995; Krishnamurti et al. 2013). Furthermore, MDs seem to have some similarity with the early stages of hurricane

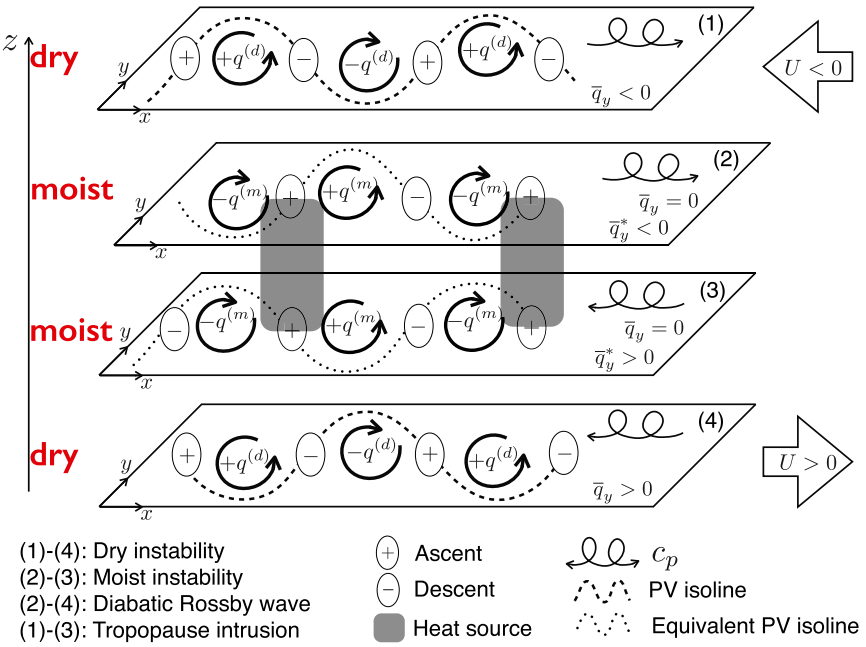

FIG. A1. As in Fig. 3, but for a basic state with easterly vertical shear.

development. Both hurricanes and MDs consist of upright columns of PV that extend from the surface to the upper troposphere, and the cold core seen in MDs is also evident in the early stages of hurricane development. So perhaps MDs are simply tropical depressions that form in monsoon regions. Some studies have assumed that MD genesis is fostered by the same environmental conditions that foster tropical cyclogenesis (Prajeesh et al. 2013), but further work is needed to go beyond such empirical descriptions and understand the growth mechanism.

Acknowledgments. Both authors acknowledge support by Office of Naval Research Awards N00014-11-1-0617 and N00014-15-1-2531 and National Science Foundation Award AGS-1253222. We thank Maxi Böttcher and Wernli Heini from Eidgenössische Technische Hochschule (ETH) Zürich, Switzerland, for providing their DRW track data. We also thank Adam Sobel, David Raymond, and one anonymous reviewer for the thoughtful suggestions and insightful comments, which helped us bring this paper into its final form. WRB thanks Kerry Emanuel, Brian Farrell, and Paul O'Gorman for helpful discussions. ERA-Interim data were obtained from the Research Data Archive that is maintained by the Computational and Information Systems Laboratory at the National Center for Atmospheric Research (NCAR). NCAR is sponsored by the National Science Foundation. The data are available at http://rda.ucar.edu.

APPENDIX

Interactions of PV Components in Mean Easterly Vertical Shear

The main text reviewed mechanisms of baroclinic instability in a basic state with westerly vertical shear; here we present a schematic (Fig. A1) showing how the various CRWs behave in easterly vertical shear, which characterizes the mean state in which MDs evolve. Changing the sign of the vertical shear from positive to negative shifts ascent from the east to the west side of cyclonic PV anomalies and, thus, reverses the intrinsic direction of propagation of the moist CRWs in the two middle layers (cf. Fig. 3). Mathematically, this occurs because $\overline{q}^*_y$ changes sign, owing to the sign operator in (9). The sign of $\overline{q}_y$ also reverses compared to the westerly shear case; this occurs in the bottom layer because the meridional temperature gradient, being on the bottom boundary, serves as a meridional PV gradient (Bretherton 1966), and the temperature gradient must change sign to maintain thermal wind balance. However, the change in sign of $\overline{q}_y$ in the top layer requires either treating this layer as an upper boundary on which the temperature gradient acts like a (negative) PV gradient or assuming that the easterly vertical shear is strong enough to change the sign of the actual interior meridional PV gradient. In contrast, in westerly shear $\overline{q}_y$ could be simply taken to represent the meridional gradient of planetary vorticity (i.e., β). Wang (1990)

discusses this asymmetry between easterly and westerly vertical shear. If we do not assume an upper boundary exists and do not assume that the easterly shear is strong enough to overcome β, then dry CRWs in the top layer will propagate westward relative to the flow and there will be no dry baroclinic instability nor an unstable ''tropopause intrusion'' mode. An additional unstable interaction between CRWs in layers 1 and 2 would then become possible, but we speculate that this may not be physically realizable because moist convective heating will be weak because of specific humidities being very low in this upper-tropospheric part of the domain. The two other modes—namely, the diabatic Rossby wave and the interior moist instability mode—remain unstable regardless of the sign of the PV gradient in the top layer.

REFERENCES

Ajayamohan, R. S., W. J. Merryfield, and V. V. Kharin, 2010: Increasing trend of synoptic activity and its relationship with extreme rain events over central India. *J. Climate*, **23**, 1004–1013, doi:10.1175/2009JCLI2918.1.

Boettcher, M., and H. Wernli, 2011: Life cycle study of a diabatic Rossby wave as a precursor to rapid cyclogenesis in the North Atlantic—Dynamics and forecast performance. *Mon. Wea. Rev.*, **139**, 1861–1878, doi:10.1175/2011MWR3504.1.

——, and ——, 2013: A 10-yr climatology of diabatic Rossby waves in the Northern Hemisphere. *Mon. Wea. Rev.*, **141**, 1139–1154, doi:10.1175/MWR-D-12-00012.1.

Boos, W. R., J. V. Hurley, and V. S. Murthy, 2015: Adiabatic westward drift of Indian monsoon depressions. *Quart. J. Roy. Meteor. Soc.*, **141**, 1035–1048, doi:10.1002/qj.2454.

——, B. E. Mapes, and V. S. Murthy, 2016: Potential vorticity structure and propagation mechanism of Indian monsoon depressions. *The Global Monsoon System*, C.-P. Chang et al., Eds., World Scientific Series on Asia-Pacific Weather and Climate, World Scientific, in press.

Bretherton, F. P., 1966: Baroclinic instability and the short wavelength cut-off in terms of potential vorticity. *Quart. J. Roy. Meteor. Soc.*, **92**, 335–345, doi:10.1002/qj.49709239303.

Charney, J., and M. Stern, 1962: On the stability of internal baroclinic jets in a rotating atmosphere. *J. Atmos. Sci.*, **19**, 159–172, doi:10.1175/1520-0469(1962)019<0159:OTSOIB>2.0.CO;2.

Cohen, N. Y., and W. R. Boos, 2014: Has the number of Indian summer monsoon depressions decreased over the last thirty years? *Geophys. Res. Lett.*, **41**, 7846–7853, doi:10.1002/2014GL061895.

Dee, D. P., and Coauthors, 2011: The ERA-Interim reanalysis: Configuration and performance of the data assimilation system. *Quart. J. Roy. Meteor. Soc.*, **137**, 553–597, doi:10.1002/qj.828.

de Vries, H., J. Methven, T. H. A. Frame, and B. J. Hoskins, 2010: Baroclinic waves with parameterized effects of moisture interpreted using Rossby wave components. *J. Atmos. Sci.*, **67**, 2766–2784, doi:10.1175/2010JAS3410.1.

Ding, Y., and D. R. Sikka, 2006: Synoptic systems and weather. *The Asian Monsoon*, B. Wang, Ed., Springer, 131–201.

Douglas, M. W., 1992: Structure and dynamics of two monsoon depressions. Part I: Observed structure. *Mon. Wea. Rev.*, **120**, 1524–1547, doi:10.1175/1520-0493(1992)120<1524:SADOTM>2.0.CO;2.

Emanuel, K. A., 1991: A scheme for representing cumulus convection in large-scale models. *J. Atmos. Sci.*, **48**, 2313–2329, doi:10.1175/1520-0469(1991)048<2313:ASFRCC>2.0.CO;2.

——, M. Fantini, and A. J. Thorpe, 1987: Baroclinic instability in an environment of small stability to slantwise moist convection. Part I: Two-dimensional models. *J. Atmos. Sci.*, **44**, 1559–1573, doi:10.1175/1520-0469(1987)044<1559:BIIAEO>2.0.CO;2.

——, J. D. Neelin, and C. S. Bretherton, 1994: On large-scale circulations in convecting atmospheres. *Quart. J. Roy. Meteor. Soc.*, **120**, 1111–1143, doi:10.1002/qj.49712051902.

Farrell, B., 1982: The initial growth of disturbances in a baroclinic flow. *J. Atmos. Sci.*, **39**, 1663–1686, doi:10.1175/1520-0469(1982)039<1663:TIGODI>2.0.CO;2.

——, 1985: Transient growth of damped baroclinic waves. *J. Atmos. Sci.*, **42**, 2718–2727, doi:10.1175/1520-0469(1985)042<2718:TGODBW>2.0.CO;2.

Fjørtoft, R., 1950: Application of integral theorems in deriving criteria of stability for laminar flows and for the baroclinic circular vortex. *Geofys. Publ.*, **17**, 5–52.

Godbole, R., 1977: The composite structure of the monsoon depression. *Tellus*, **29**, 25–40, doi:10.1111/j.2153-3490.1977.tb00706.x.

Goswami, B., R. Keshavamurty, and V. Satyan, 1980: Role of barotropic, baroclinic and combined barotropic-baroclinic instability for the growth of monsoon depressions and midtropospheric cyclones. *J. Earth Syst. Sci.*, **89**, 79–97.

Grotjahn, R., 2003: Baroclinic instability. *Encyclopedia of Atmospheric Sciences*, J. R. Holton, J. A. Curry, and J. A. Pyle, Eds., Academic Press, 419–467.

Heifetz, E., C. H. Bishop, B. J. Hoskins, and J. Methven, 2004: The counter-propagating Rossby-wave perspective on baroclinic instability. I: Mathematical basis. *Quart. J. Roy. Meteor. Soc.*, **130**, 211–231, doi:10.1002/qj.200413059610.

Holton, J. R., and G. J. Hakim, 2013: *An Introduction to Dynamic Meteorology*. Academic Press, 552 pp.

Hurley, J. V., and W. R. Boos, 2015: The global distribution of monsoon depressions. *Quart. J. Roy. Meteor. Soc.*, **141**, 1049–1064, doi:10.1002/qj.2447.

India Meteorological Department, 2011: Tracks of cyclones and depressions over north Indian Ocean (from 1891 onwards). India Meteorological Department Tech. Note, 48 pp.

Keshavamurty, R., G. Asnani, P. Pillai, and S. Das, 1978: Some studies of the growth of monsoon disturbances. *Proc. Indian Acad. Sci., Earth Planet. Sci.*, **87**, 61–75.

Krishnakumar, V., R. Keshavamurty, and S. Kasture, 1992: Moist baroclinic instability and the growth of monsoon depressions—Linear and nonlinear studies. *Proc. Indian Acad. Sci., Earth Planet. Sci.*, **101**, 123–152.

Krishnamurti, T. N., 1985: Summer Monsoon Experiment—A review. *Mon. Wea. Rev.*, **113**, 1590–1626, doi:10.1175/1520-0493(1985)113<1590:SMER>2.0.CO;2.

——, J. Molinari, and H. L. Pan, 1976: Numerical simulation of the Somali jet. *J. Atmos. Sci.*, **33**, 2350–2362, doi:10.1175/1520-0469(1976)033<2350:NSOTSJ>2.0.CO;2.

——, A. Martin, R. Krishnamurti, A. Simon, A. Thomas, and V. Kumar, 2013: Impacts of enhanced CCN on the organization of convection and recent reduced counts of monsoon depressions. *Climate Dyn.*, **41**, 117–134, doi:10.1007/s00382-012-1638-z.

Landsea, C. W., and J. L. Franklin, 2013: Atlantic hurricane database uncertainty and presentation of a new database format. *Mon. Wea. Rev.*, **141**, 3576–3592, doi:10.1175/MWR-D-12-00254.1.

——, and Coauthors, 2004: The Atlantic Hurricane Database Reanalysis Project: Documentation for the 1851–1910 alterations

and additions to the HURDAT database. *Hurricanes and Typhoons: Past, Present, and Future*, R. J. Murnane and K.-B. Liu, Eds., Columbia University Press, 177–221.

Lighthill, M. J., 1963: Boundary layer theory. *Laminar Boundary Layers*, L. Rosenhead, Ed., Oxford University Press, 46–113.

Lindzen, R., B. Farrell, and A. Rosenthal, 1983: Absolute barotropic instability and monsoon depressions. *J. Atmos. Sci.*, **40**, 1178–1184, doi:10.1175/1520-0469(1983)040<1178:ABIAMD>2.0.CO;2.

Mak, M., 1983: A moist baroclinic model for monsoonal mid-tropospheric cyclogenesis. *J. Atmos. Sci.*, **40**, 1154–1162, doi:10.1175/1520-0469(1983)040<1154:AMBMFM>2.0.CO;2.

McTaggart-Cowan, R., G. D. Deane, L. F. Bosart, C. A. Davis, and T. J. Galarneau Jr., 2008: Climatology of tropical cyclogenesis in the North Atlantic (1948–2004). *Mon. Wea. Rev.*, **136**, 1284–1304, doi:10.1175/2007MWR2245.1.

——, T. J. Galarneau Jr., L. F. Bosart, R. W. Moore, and O. Martius, 2013: A global climatology of baroclinically influenced tropical cyclogenesis. *Mon. Wea. Rev.*, **141**, 1963–1989, doi:10.1175/MWR-D-12-00186.1.

Mishra, S., and P. Salvekar, 1980: Role of baroclinic instability in the development of monsoon disturbances. *J. Atmos. Sci.*, **37**, 383–394, doi:10.1175/1520-0469(1980)037<0383:ROBIIT>2.0.CO;2.

Montgomery, M. T., and B. F. Farrell, 1991: Moist surface frontogenesis associated with interior potential vorticity anomalies in a semigeostrophic model. *J. Atmos. Sci.*, **48**, 343–368, doi:10.1175/1520-0469(1991)048<0343:MSFAWI>2.0.CO;2.

Mooley, D. A., and J. Shukla, 1987: Characteristics of the westward-moving summer monsoon low pressure systems over the Indian region and their relationship with the monsoon rainfall. University of Maryland Center for Ocean–Land–Atmosphere Interactions Tech. Rep., 218 pp.

Moore, R. W., and M. T. Montgomery, 2004: Reexamining the dynamics of short-scale, diabatic Rossby waves and their role in midlatitude moist cyclogenesis. *J. Atmos. Sci.*, **61**, 754–768, doi:10.1175/1520-0469(2004)061<0754:RTDOSD>2.0.CO;2.

——, ——, and H. Davies, 2013: Genesis criteria for diabatic Rossby vortices: A model study. *Mon. Wea. Rev.*, **141**, 252–263, doi:10.1175/MWR-D-12-00080.1.

Moorthi, S., and A. Arakawa, 1985: Baroclinic instability with cumulus heating. *J. Atmos. Sci.*, **42**, 2007–2031, doi:10.1175/1520-0469(1985)042<2007:BIWCH>2.0.CO;2.

Parija, N. R., and S. K. Dash, 1995: Some aspects of the characteristics of monsoon disturbances using a combined barotropic-baroclinic model. *Adv. Atmos. Sci.*, **12**, 487–506, doi:10.1007/BF02657007.

Parker, D. J., and A. J. Thorpe, 1995: Conditional convective heating in a baroclinic atmosphere: A model of convective frontogenesis. *J. Atmos. Sci.*, **52**, 1699–1711, doi:10.1175/1520-0469(1995)052<1699:CCHIAB>2.0.CO;2.

Pedlosky, J., 1987: *Geophysical Fluid Dynamics*. Springer, 710 pp.

Pierrehumbert, R., 1995: Baroclinic instability. *Annu. Rev. Fluid Mech.*, **27**, 419–467, doi:10.1146/annurev.fl.27.010195.002223.

Plant, R. S., G. C. Craig, and S. L. Gray, 2003: On a threefold classification of extratropical cyclogenesis. *Quart. J. Roy. Meteor. Soc.*, **129**, 2989–3012, doi:10.1256/qj.02.174.

Prajeesh, A. G., K. Ashok, and D. V. B. Rao, 2013: Falling monsoon depression frequency: A Gray-Sikka conditions perspective. *Sci. Rep.*, **3**, 2989, doi:10.1038/srep02989.

Rajendra Kumar, J., and S. K. Dash, 2001: Interdecadal variations of characteristics of monsoon disturbances and their epochal relationships with rainfall and other tropical features. *Int. J. Climatol.*, **21**, 759–771, doi:10.1002/joc.628.

Rao, K., and S. Rajamani, 1970: Diagnostic study of a monsoon depression by geostrophic baroclinic model. *Indian J. Meteor. Hydrol. Geophys.*, **21**, 187–194.

Raymond, D., and H. Jiang, 1990: A theory for long-lived mesoscale convective systems. *J. Atmos. Sci.*, **47**, 3067–3077, doi:10.1175/1520-0469(1990)047<3067:ATFLLM>2.0.CO;2.

Saha, K., and C. Chang, 1983: The baroclinic processes of monsoon depressions. *Mon. Wea. Rev.*, **111**, 1506–1514, doi:10.1175/1520-0493(1983)111<1506:TBPOMD>2.0.CO;2.

Sanders, F., 1984: Quasi-geostrophic diagnosis of the monsoon depression of 5–8 July 1979. *J. Atmos. Sci.*, **41**, 538–552, doi:10.1175/1520-0469(1984)041<0538:QGDOTM>2.0.CO;2.

——, and B. J. Hoskins, 1990: An easy method for estimation of Q-vectors from weather maps. *Wea. Forecasting*, **5**, 346–353, doi:10.1175/1520-0434(1990)005<0346:AEMFEO>2.0.CO;2.

Shukla, J., 1977: Barotropic-baroclinic instability of mean zonal wind during summer monsoon. *Pure Appl. Geophys.*, **115**, 1449–1461, doi:10.1007/BF00874418.

——, 1978: CISK-barotropic-baroclinic instability and the growth of monsoon depressions. *J. Atmos. Sci.*, **35**, 495–508, doi:10.1175/1520-0469(1978)035<0495:CBBIAT>2.0.CO;2.

Sikka, D. R., 1977: Some aspects of the life history, structure and movement of monsoon depressions. *Pure Appl. Geophys.*, **115**, 1501–1529, doi:10.1007/BF00874421.

——, 2006: A study on the monsoon low pressure systems over the Indian region and their relationship with drought and excess monsoon seasonal rainfall. Center for Ocean–Land–Atmosphere Studies Tech. Rep. 217, 61 pp.

Snyder, C., and R. S. Lindzen, 1991: Quasi-geostrophic wave-CISK in an unbounded baroclinic shear. *J. Atmos. Sci.*, **48**, 76–86, doi:10.1175/1520-0469(1991)048<0076:QGWCIA>2.0.CO;2.

Sobel, A. H., J. Nilsson, and L. M. Polvani, 2001: The weak temperature gradient approximation and balanced tropical moisture waves. *J. Atmos. Sci.*, **58**, 3650–3665, doi:10.1175/1520-0469(2001)058<3650:TWTGAA>2.0.CO;2.

Vallis, G. K., 2006: *Atmospheric and Oceanic Fluid Dynamics: Fundamentals and Large-Scale Circulation.* Cambridge University Press, 745 pp.

Wang, B., 1990: On the asymmetry of baroclinic instability between easterly and westerly shear. *Tellus*, **42A**, 463–468, doi:10.1034/j.1600-0870.1990.t01-3-00005.x.

Yano, J.-I., and K. Emanuel, 1991: An improved model of the equatorial troposphere and its coupling with the stratosphere. *J. Atmos. Sci.*, **48**, 377–389, doi:10.1175/1520-0469(1991)048<0377:AIMOTE>2.0.CO;2.

Yoon, J., and T. Chen, 2005: Water vapor budget of the Indian monsoon depression. *Tellus*, **57A**, 770–782, doi:10.1111/j.1600-0870.2005.00145.x.